CHALMERS
UNIVERSITY OF TECHNOLOGY

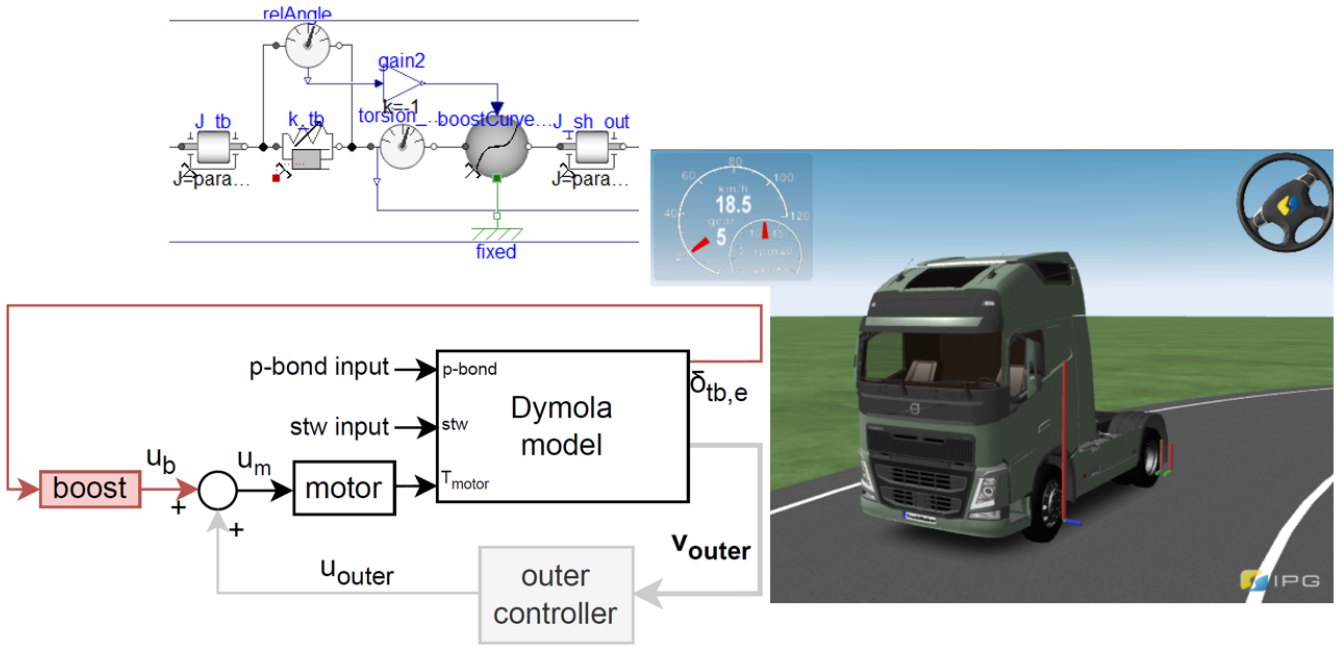

Modelling and control of active power steering systems for heavy trucks

Master's thesis in Systems, Control and Mechatronics

Sharath Chandra Ashok Kumar
Emil Erikmats

DEPARTMENT OF ELECTRICAL ENGINEERING

DEPARTMENT OF MECHANICS AND MARITIME SCIENCES

CHALMERS UNIVERSITY OF TECHNOLOGY
Gothenburg, Sweden 2023
www.chalmers.se

Master's thesis 2023

Modelling and control of active power steering systems for heavy trucks

Sharath Chandra Ashok Kumar
Emil Erikmats

CHALMERS
UNIVERSITY OF TECHNOLOGY

Department of Electrical Engineering
Division of Systems and Control
Department of Mechanics and Maritime Sciences
Division of Vehicle Engineering and Autonomous Systems
Chalmers University of Technology
Gothenburg, Sweden 2023

Modelling and control of active power steering systems for heavy trucks

SHARATH CHANDRA ASHOK KUMAR
EMIL ERIKMATS

Supervisors:
Alireza Marzbanrad, Combine
Examiners:
Balázs Adam Kulcsár, Department of Electrical Engineering
Bengt J H Jacobson, Department of Mechanics and Maritime Sciences

Master's Thesis 2023
Department of Electrical Engineering, Division of Systems and Control
Department of Mechanics and Maritime Sciences, Division of Vehicle Engineering and Autonomous Systems
Chalmers University of Technology
SE-412 96 Gothenburg
Telephone +46 31 772 1000

Cover: Model of hydraulic gearbox, control block diagram and IPG TruckMaker simulation.

Typeset in LaTeX
Gothenburg, Sweden 2023

Modelling and control of active power steering systems for heavy trucks

SHARATH CHANDRA ASHOK KUMAR
EMIL ERIKMATS
Department of Electrical Engineering
Department of Mechanics and Maritime Sciences
Chalmers University of Technology

Abstract

Transportation via trucks constitutes an important part of the logistics chain. Today's trucks can take a front axle load of approximately 8 tonnes. To be able to maneuver at high front axle loads, the driver needs assistance from additional power sources. The additional power can be provided through different sources in different steering topologies: Hydraulic Power Steering (HPS), Electric Power Steering (EPS) or Electro-Hydraulic Power Steering (EHPS), where HPS and EHPS are more common today. Some benefits of EPS over the other two are reduced energy consumption, improved autonomous drivability, and the absence of hydraulic oils which can contaminate soil, groundwater and seawater. However, hydraulics are faster than electromechanical systems.
This thesis aims to see if acceptable steering performance can be achieved with EPS and compare it to EHPS by modelling, designing controllers and simulating the complete vehicle-driver-ground systems. The version of EHPS chosen was a Volvo Dynamic Steering-like (VDS-like) topology. The mechanical systems were mainly modeled using tools in Dymola but also in MATLAB, Simulink, and TruckMaker for Simulink (TM4SL) environment. The Dymola model of the VDS-like model was validated by comparing it to Volvo's steering black box model at Chalmers. The control was developed in MATLAB and Simulink, where PID controller was selected for the motor and the outer control scheme being $\mathcal{H}_2$ for energy optimization. The mechanical system, the motor model, and the controllers were then connected in TM4SL. Evaluation on TruckMaker was conducted by simulating two scenarios namely, path following in a figure of eight and in a wheel lock scenario.
The models of the two steering systems developed were found to be acceptable while the designed boost for the EPS system also performed supportively. The controller however did not produce the anticipated behaviour.

Keywords: Power steering system, Electric Power Steering system (EPS), Electro-Hydraulic Power Steering system (EHPS), Robust and Nonlinear Control.

Acknowledgements

We would like to express our deepest gratitude to the following individuals and organizations who have played a significant role in the completion of this thesis:

Alireza Marzbanrad
We are immensely thankful to our thesis advisor, Alireza Marzbanrad, for his unwavering support, guidance, and invaluable insights throughout the thesis process.

Bengt J H Jacobson and **Balázs Adam Kulcsár**
We extend our appreciation to both our examiners at Chalmers, for providing access to resources, their valuable feedback, encouragement and guidance, which greatly enhanced the quality of this thesis.

Filip Petersson and **Combine AB**
We thank Filip and Combine at large for ensuring the necessary supportive environment and facilities was available during our stint there.

Lastly, a thanks to **IPG Automotive** and **Aria Noori** for their immense support to get us up to speed with IPG TruckMaker.

Sharath Chandra Ashok Kumar & Emil Erikmats, Gothenburg, November, 2023

List of Acronyms

Below is the list of acronyms that have been used throughout this thesis listed in alphabetical order:

HPS	Hydraulic Power Steering
EHPS	Electr-Hydraulic Power Steering
EPS	Electric Power Steering
ADAS	Advanced Driver Assist Systems
AOR	Axis Of Rotation
CCW	Counter Clock Wise
CW	Clock Wise
FMU	Functional Mock-up Unit
ICE	Internal Combustion Engine
LLSE	Linear Least Squares Estimate
WRT	With respect to
TM	TruckMaker
GUI	Graphical User Interface

Nomenclature

Below is the nomenclature of variables that have been used throughout this thesis.

B_e	Electric boost curve emulating the hydraulic one in Nm
B_h	Hydraulic boost curve in Nm
D_{dl}	Drag link damping in Nms
$c_{lin,non}$	Linear spring constant of the torsion bar's nonlinear region in N/m
c_{lin}	Linear spring constant of the torsion bar's linear region in N/m
δ_{kn}	Knuckle angle in rad
δ_{pa}	Pitman arm angle in rad
$\delta_{tb,e}$	Angle displacement of the electrical torsion bar in rad
$\delta_{tb,0}$	Displacement angle where the nonlinear torsion bar transitions from linear to nonlinear region in rad
$\delta_{tb,h}$	Angle displacement of the hydraulics torsion bar in rad
$\ddot{\delta}_{kn}$	Angular acceleration of knuckle in rad/s^2
F_R, F_L	Forces on suspension, left and right in N
F_{buff}	Force that acts when wheel angle has reached maximum wheel turn position in N
$\phi_{rel,T}$	Deflection angle of the nonlinear torsion bar, resulting in torque (offset in relaxed state subtracted) in rad
$\gamma_{e,1}$	Constant multiplied with the linear term of the third order polynomial electric boost curve
$\gamma_{e,2}$	Constant multiplied with the squared term of the third order polynomial electric boost curve
$\gamma_{e,3}$	Constant multiplied with the cubed term of the third order polynomial electric boost curve
$\gamma_{h,1}$	Constant multiplied with the linear term of the third order polynomial hydraulic boost curve
$\gamma_{h,2}$	Constant multiplied with the squared term of the third order polynomial hydraulic boost curve
$\gamma_{h,3}$	Constant multiplied with the cubed term of the third order polynomial hydraulic boost curve
i_{wr}	Gear ratio of the worm gear in m/rad
i_{em}	Gear ratio of the electric motor's gearbox. Unitless

K_{dl}	Spring constant of drag link in N/m
L_{pa}	Length of pitman arm in m
m_{axle}	Mass of axle in kg
ω_n	Frequency of oscillation
ω_{kn}	Angular velocity of knuckle in rad/s
ω_{pa}	Angular velocity of pitman arm in rad/s
$T_{k,tb}$	Torsion bar spring torque in Nm
w_p	weighting of the power bond input to the main plant
w_{stw}	weighting of the steering wheel input to the main plant
w_{inf}	weighting of the $\mathcal{H}_\infty$ related performance outputs from the Dymola plant
w_2	weighting of the $\mathcal{H}_2$ related performance outputs from the Dymola plant
z_{inf}	Performance outputs related to $\mathcal{H}_\infty$ control
z_2	Performance outputs related to $\mathcal{H}_2$ control
u_{outer}	Control signal from the outer control loop
v_{outer}	Measured outputs from the Dymola plant
ζ	Damping coefficient

Contents

1
Introduction

Transportation via trucks constitutes an important link of the logistics chain. The year of 2021 saw trucks transport 492 million metric tonnes for a total of 3.4 billion kilometers in Sweden [1]. The average truck weight for heavy trucks was 11 metric tonnes (above 3.5 tonnes is considered heavy [1]). These heavy trucks naturally have high axle loads when fully loaded, with the front steering axle bearing loads of up to eight tonnes in extreme cases [2]–[6]. The steering system for trucks is thus distinctive from cars because of the loads/forces the steering axle and the entire steering system is exposed to.

1.1 Background

The steering system is the interconnection of shafts, linkages, gears, hydraulics and motors which serves the purpose of controlling the direction of the vehicle. The non-assisted steering system demands the raw physical effort of driver to steer. As the Payload capacity of trucks increased, so did the requirement of easing the driver's effort to steer. Further, with increased emphasis on safety, the steering systems were developed to exhibit Advanced Driver Assist Systems (ADAS) capabilities. In this section, the evolution of steering is presented.

1.1.1 Manual Steering

It is essential to know about the basic steering system components considered in this thesis and their functionality such that the developments in the steering system can be recognized. The following components are considered basic steering system components:

- **Steering Wheel** is the driver's interface with the steering system to help the driver guide the vehicle in the intended path. With the absence of power assist, these steering wheels were larger in circumference in order to make it easy for the driver to apply larger torques to achieve the required steering maneuver.
- **Steering Column and shaft** is a *fixed* or *flexible* shaft connecting the steering wheel to the steering gearbox. This shaft is responsible for firstly, transmitting torque applied by the driver. Secondly, to compensate for angle and length changes in column in case of driver height adjustable column or tilt cabs.

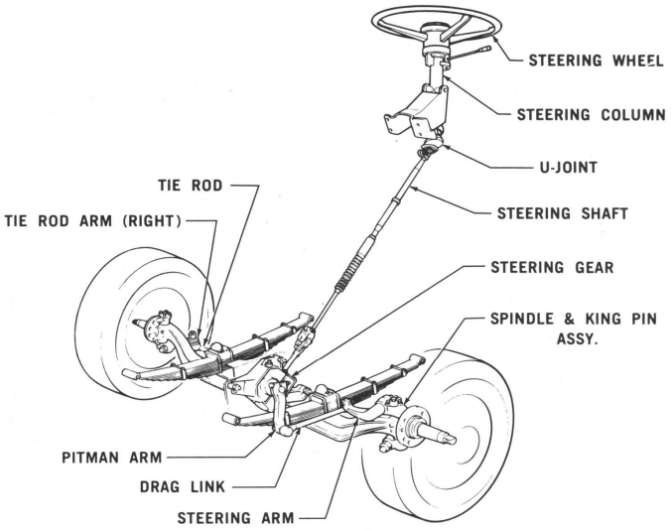

Figure 1.1: Manual Steering [7]

- **Gearbox** is either a *worm and roller* or *recirculating ball* type arrangement used to amplify the steering torque exerted by the driver. In this process of amplification, the input rotational motion from the driver is converted to a rotational motion at the pitman arm and thereby a translation motion at the draglink.
- **Pitman arm** is a link responsible for converting the torque from the gearbox to a force acting on the drag link.
- **Drag link** connects the pitman arm with the steering arm with force from pitman arm transmitted through ball joints.
- **Steering Arm** is responsible for converting the drag link force to a moment about the kingpin.
- **Tie rod** is of tubular make connecting the left and right wheels and hence transferring force between them.

Pure manual steering hence relies entirely on the effort put in by the driver to steer.

1.1.2 Hydraulic Power Steering

In order to reduce the efforts put in by the driver to steer, hydraulics is incorporated into the steering system. All the parts explained in the previous system have been carried forward and only the new parts that define a hydraulic power steering are explained.

- **Pump and Reservoir** are an integral unit that is belt driven and consumes power from the engine at all times. At high engine speeds, the pressure developed by the pump increases to levels that far exceed the capacity needed to steer thus calling for the reinforcement of components downstream of the pump. To avoid this, *flow control valves* are made use of. These valves redirect the excess fluid back into the reservoir which stores the steering fluid.

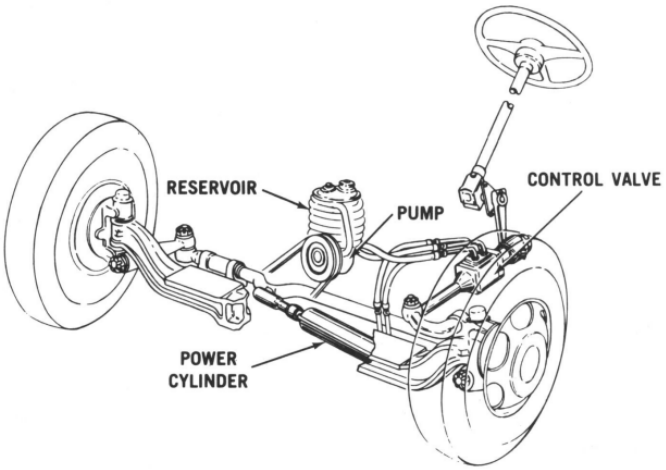

Figure 1.2: Hydraulic Power Steering [7]

- **Control Valve** obtains hydraulic fluid under pressure from the pump which channels it to the power cylinder to provide the mechanical boost as required to support the steering maneuver. The valve opening increases proportional (usually of the degree 2 or 3) to the effort needed to steer and stabilizes at a point that is sufficient to provide the necessary boost and assist. Hence, the operation can be summarized to be of a hydraulic Wheatstone bridge.

With hydraulics assisting the driver, the effort demanded by the steering system is reduced thus making it easy for the driver in maneuvering the truck. As another advantage, the steering wheel size is reduced making more room in the cabin and improving ergonomics.

1.1.3 Electro-Hydraulic Power Steering

Implementation of an Electro-Hydraulic power steering system can be categorized into two. First, a system where in the hydraulic pump associated to steering is independent of the engine(figure 1.3). Second, the hydraulic pump is belt-fed from the engine but additionally, a motor is attached to the steering gearbox(figure 1.4). From the thesis perspective, the implementation introduced latter will be considered as the EHPS. What follows is the explanation of the two implementations introduced in this subsection while still considering the parts explained in the HPS to be applicable.

1.1.3.1 Hydraulic pump powered by motor

As the name suggests, this is a steering system where the hydraulic pump is independent of the engine. The hydraulic pump is instead powered by an electric motor connected to the battery. The behaviour of the system as seen from the driver emulates the exact behaviour as that of pure hydraulic power steering. This decoupling of the pump and engine implies that the pump is driven only when necessary and at its highest efficient operating point.

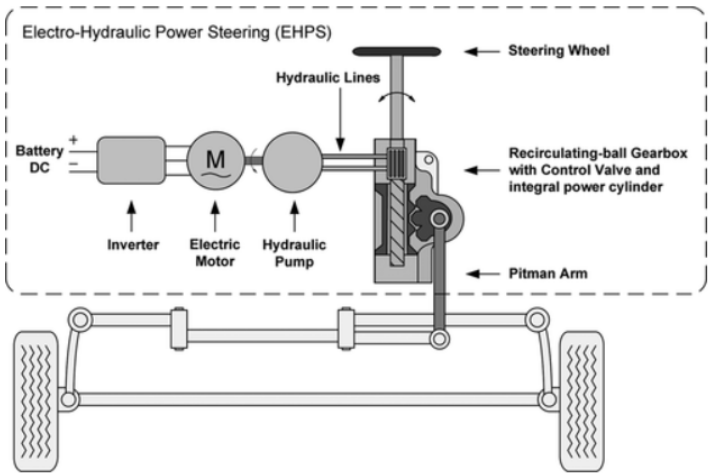

Figure 1.3: Hydraulic pump powered by motor [8]

1.1.3.2 Hydraulic gearbox with motor attachment

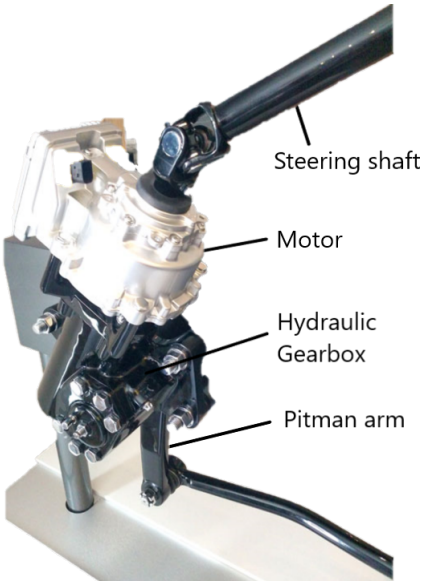

Figure 1.4: Hydraulic gearbox with motor attachment [9]

With the hydraulic gearbox providing the steering assist which results in reduced steering effort, the motor assists in providing additional torque based on driver input to make the steering more responsive, comfortable and improve directional stability. The transition observed here is from reducing driver effort to improving driver comfort while also emphasising on driver assist functions.

- **Steering Angle Sensor** detects position of steering wheel which is used by the ECU for other computations related to driver assist.
- **Torsion Bar** is made of tempered steel, having a lower stiffness compared to the rest of the system, is employed to estimate the torque applied to the steering wheel. Under ideal circumstances, where no friction exists between

the steering wheel and the torsion bar, the torsion bar torque is equivalent to the steering wheel torque. The torsion bar is linked to the spindle, which transforms rotation into a linear motion of the piston within the steering house. This is explained in detain in figure 2.5.

- **Electronic Control Unit** is the main computer taking in data from relevant vehicle sensors to compute the assist and functionality of motor in general that must be delivered.
- **Motor** provides the torque required for the driver assist functionality. The primary goal of the motor is to improve the overall driving comfort by helping in directional stability, reducing steering jerks due to bad road conditions and improving maneuverability of steering at low vehicle speeds. Essentially, assisting driver in disturbance rejection.

What distinguishes the former from the latter implementation of EHPS is that in the latter, the motor is dedicated to provide driver assistance to help in disturbance rejection (additionally, where active safety features can be executed) as opposed to just powering the hydraulic pump.

1.1.4 Electric Power Steering

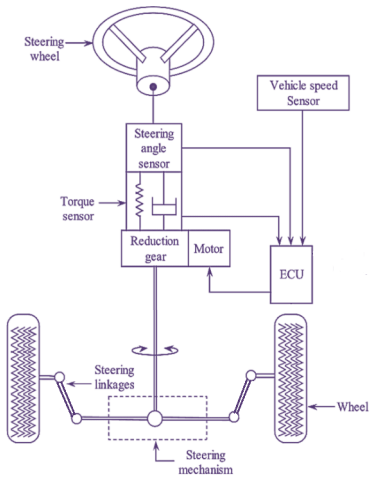

Figure 1.5: Electric Power Steering [10]

A pure electric steering system designed by eliminating the hydraulics as seen earlier while retaining the motor. This design makes use of a torsion bar and a reduction gear additionally.

- **Torque Sensor** provides the measurement of driver input effort to maneuver the truck. This acts as a reference for the assist torque that motor delivers.
- **Motor** is required to provide the same functionality as explained in the previous section. Additionally, with the absence of hydraulic torque assistance, the motor must be capable of delivering higher torques to support the driving

operation. Hence, this motor must have a higher output rating as opposed to that presented earlier.

- **Reduction Gear** is a dedicated gearbox that links motor to the steering system. The sole purpose of it is to reduce motor speed and increase torque while also helping in maintaining accurate position.

The benefit of this topology over the others is its flexibility in operation. The ECU can adjust the steering feel, behavior and power assist based on individual driver preferences, driving condition, etc, thus enabling a customized steering experience. Also, it paves the way for many of the ADAS features to be incorporated into steering which improves overall safety.

1.2 Objectives

The objective of this Master's thesis is to design a controller for the VDS-like topology and subsequently, a satisfactory model including the control aspect of an EPS topology. They should be similar enough for a valid comparison between the two said topologies. The control aspect is affected by the design approach of the controllers which therefore also becomes a question this thesis aims to answer. The research questions are therefore in short:

1. For a heavy duty truck, how can the dynamics of an EPS and VDS-like topology be designed and satisfactorily modeled?
2. Can any analytical conclusions about the behaviour of the steering models be drawn from the comparison with a steering model provided by industry.
3. Considering a $\mathcal{H}_2$ optimal controller, how can such a controller be implemented for VDS-like and EPS topologies?
4. What are the distinctive performance characteristics of EPS topology as compared to the existing VDS-like topology in terms of maneuverability (i.e., lane keeping, yaw control, torque reference control, bandwidth, etc)?

On the control front, the objective is to reject disturbance originating at the wheels and moving up the steering system such that driver effort never exceeds $4\,\mathrm{N\,m}$ in rotating the steering while the steering wheel is also stable without jitters. Also considered is the reliable steering action to counter wheel lock.

1.3 Limitations

This project will not consider the following material, methods and applications:

- Only heavy trucks with a single front axle and a kerb weight of above 3.5 metric tonnes will be considered.
- The domain of validity of the model will not be derived.
- Some time delays in the steering systems arising due to approximations in modeling of steering and motor behavior might be neglected.

- Tire dynamics, suspension dynamics, braking dynamics and the powertrain will generate dynamics seen as disturbances when developing the control algorithm. These disturbances will not be modeled in detail in the control synthesis.
- The implementations will only be tested in simulation environments and not on physical hardware.
- Simulations will only be made on scenarios in speeds of $\geq 5\,\mathrm{km/h}$ to be able to neglect the complex tire dynamics at lower speeds.
- Motor's efficiency, electrical safety, supplied voltage and power source are not considered.

1.4 Overview of the connections

A simple figure is presented to provide an overview of the connections in focus between the different subsystems that will be explained further in the report. As depicted in figure 1.6, the `Steering System` is the subsystem of the developed steering FMU, drag link and motor. `Steering Controller` is the designed $\mathcal{H}_2$ controller and the `Vhcl Control, Vhcl Suspension` are the blocks from TruckMaker. An important note here is that mechanical correctness is upheld with the right variable exchange between subsystems.

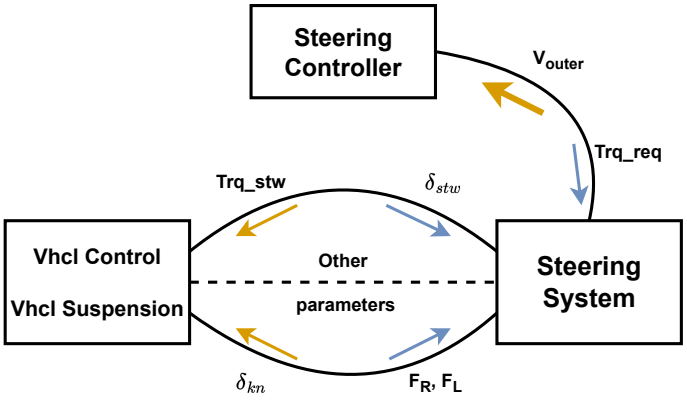

Figure 1.6: Overview of connections and interaction between different subsystems

The variables/parameters seen here will be consistent with those introduced further in the report. (F_R, F_L are forces on suspension, δ_{kn} is the knuckle angle, Trq_{stw} is the steering torque, δ_{stw} is the steering wheel angle, V_{outer} is the controller input and Trq_{req} is the request torque) `Other parameters` are for instance static torque, assist forces, steering gearbox ratio, etc., that are needed for TruckMaker to work.

1.5 Relevant UN sustainability goals

In the long run, if the new commercial vehicles are equipped with EPS, it would lead to the following benefits regarding sustainability.

One, is the absence of a need for energy supply to hydraulic pumps. The hydraulic pumps can be powered by petrol or diesel engines but also electrical sources. Energy can be dissipated as heat in its transfer from the pump, through the hydraulic system, to the actual change of movement of the steering system, leading to energy losses that could be avoided with the transition from HPS to EPS. Reducing energy consumption is in line with the seventh goal of the United Nation's (UN) Sustainable Development Goals (SDG) [11].

Secondly, the hydraulic fluids in HPS are damaging to the environment as they risk contaminating soil, groundwater and seawater [12]. This can harm humans, marine life, and terrestrial animals and plants. Since the trucks house hydraulic fluids of the power steering systems, leakage in hydraulic systems, though undesirable is inevitable which further increases the environmental and health risks. The introduction of EPS systems would therefore be beneficial in terms of the UN's 6^{th}, 12^{th}, 14^{th}, and 15^{th} SDGs [11], i.e. "*Clean water and sanitation*", "*Responsible consumption and production*", "*Life below water* " and "*Life on land*" respectively.

1.6 Thesis Outline

The thesis is structured as follows. Chapter 2 presents the modeling of both EHPS and EPS systems in Dymola along with the creation of their respective FMU's. The design of the Motor which is essential to both the steering topologies is also included. A few results from modeling can be found which is used to justify the model functionality.
Chapter 3 presents the entire control design and methodology with results justifying the controller functionality.
Chapter 4 presents the testing and verification done using IPG TruckMaker where the truck is tested on different scenarios using the developed steering model and controller.
Chapters 5 and 6 discuss the results obtained on testing and the overall findings that answer the questions presented earlier in the Objectives section.

2
Modelling

2.1 Introduction

The modelling of the system comprises all moving components between the steering wheel and the drag link. The drag link and the electric motor for the steering was modeled in Simulink. The rest was modeled in Dymola, a Modelica-based modelling and simulation program [13]. The drag link was chosen as the last mechanical component to be modeled because of the signals used in IPG TruckMaker to interface with the rest of the vehicle. More about these signals and interfacing is described in more detail in Chapter 4.

The drag link and the motor models were modeled outside the Dymola models. To be able to verify and validate the dynamics of the Dymola models, the developed Dymola models were compared to Volvo's steering black box model available at Chalmers. To be able to do that, the Dymola models were given similar inputs and outputs as the FMU provided from Chalmers. Also to note here is the model from Chalmers will be referred to as ground truth FMU in this report.

To model the steering system, already existing models explained in [14] have been used as a foundation. These models were also developed for steering system control purposes and were therefore deemed as reasonable foundations. The two systems can be seen in Figure 2.1 and 2.2, which explain the different components from the steering wheel to the pitman arm modeled.

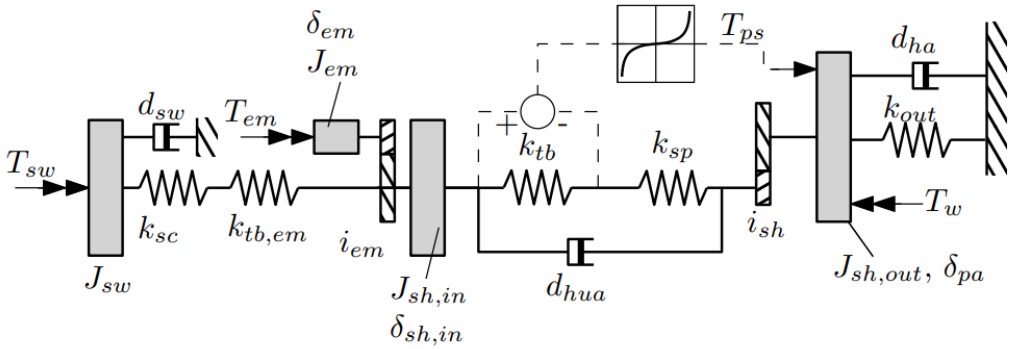

Figure 2.1: Mechanical steering system model of the VDS-like topology from [14]

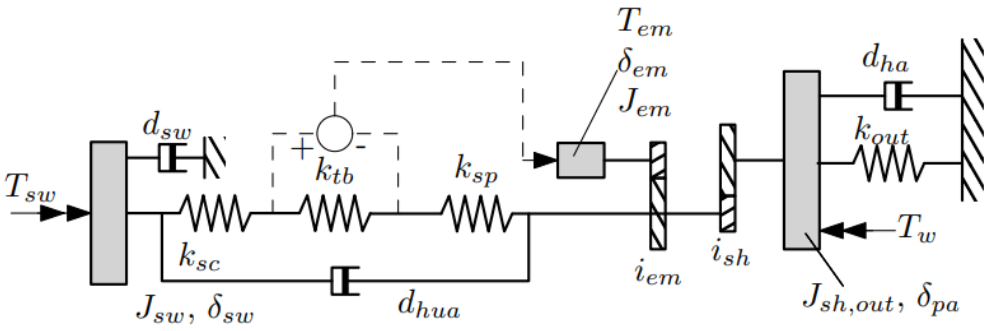

Figure 2.2: Mechanical steering system model of the EPS topology from [14].To emulate a similar behavior as the mechanical boost in Figure 2.1, a third-order polynomial is designed to use the torsion bar deflection to provide a boost torque (assist) reference to the motor.

2.2 Simplifications and assumptions

By using [14] as a baseline for the mechanical modelling, some simplifications and assumptions have been made in order to more easily be able to make a suitable controller for each topology and make it easier to compare the two:

1. The universal joints have nonlinear ratio dynamics depending on the steering wheel angle because of the nature of universal joints. However, this impact on steering dynamics is assumed to be minor and is therefore left out.
2. The steering wheel's center of gravity has an offset from its axis of rotation (AOR). And the AOR has an angular displacement from the direction of gravity, making gravity pull the steering wheel. This, so-called, steering wheel eccentricity is assumed to have a small impact on the steering and is therefore neglected.
3. All dry friction in joints, gears and along surfaces moving w.r.t each other are assumed to be small enough compared to the torques in the system to be neglected due to gear grease and hydraulic oil. Viscous friction is still considered.
4. The dynamics from the hydraulics, e.g. hydraulic fluid compression and expansions, and widening of the hoses due to pressure changes are assumed to be quick enough to be considered immediate and are therefore neglected.
5. The dynamics of the hydraulic pressure provided by the internal combustion engine (ICE) are assumed to have a small enough impact to be neglected.

Some assumptions and simplifications presented in [14] were not made in this thesis. Instead, the following decisions were made:

1. The nonlinear deflection-to-torque curve of the torsion bars' stiffness because of a saturation mechanism was considered and modeled.

2. The torsion bar's inertia is relatively small compared to the piston mass and the steering wheel inertia, resulting in high eigenfrequencies. Despite this, it's included for the steering system model to more accurately resemble a real truck steering system.

3. The spring constant k_{out} in Figure 2.1-2.2 and the well it connects to were not modeled since the truck in this thesis is expected to have the road wheels rotate noticeably. This was not the case in [14] where the road wheels were assumed to only turn with small angles and at constant speeds. Instead, torque and angular velocity inputs and outputs were modeled to be able to interface with IPG TruckMaker. The interfacing is described more in detail under chapter 4.

2.3 Modelling in Dymola

Just like in Figure 2.1 and 2.2, The Dymola models were modeled with the steering wheel to the left and the pitman-arm to the right as seen in Figure 2.3-2.4.

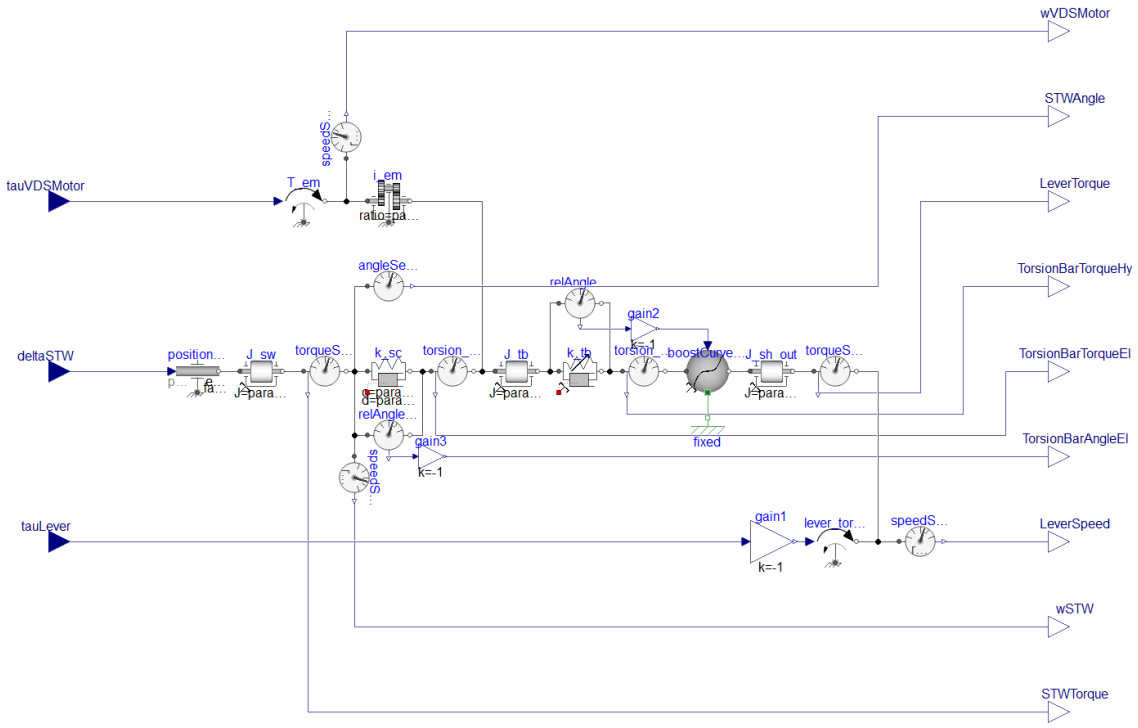

Figure 2.3: Dymola model of the VDS-like topology with steering wheel angle as input and pitman-arm torque as power bond.

2.3.1 Mechanical components

As mentioned before, the mechanical components in the Dymola model exclude the electrical motor (described in section 2.4)and the drag link (described in Chapter 4). The rest of the components are seen in Figure 2.3 and 2.4. All components

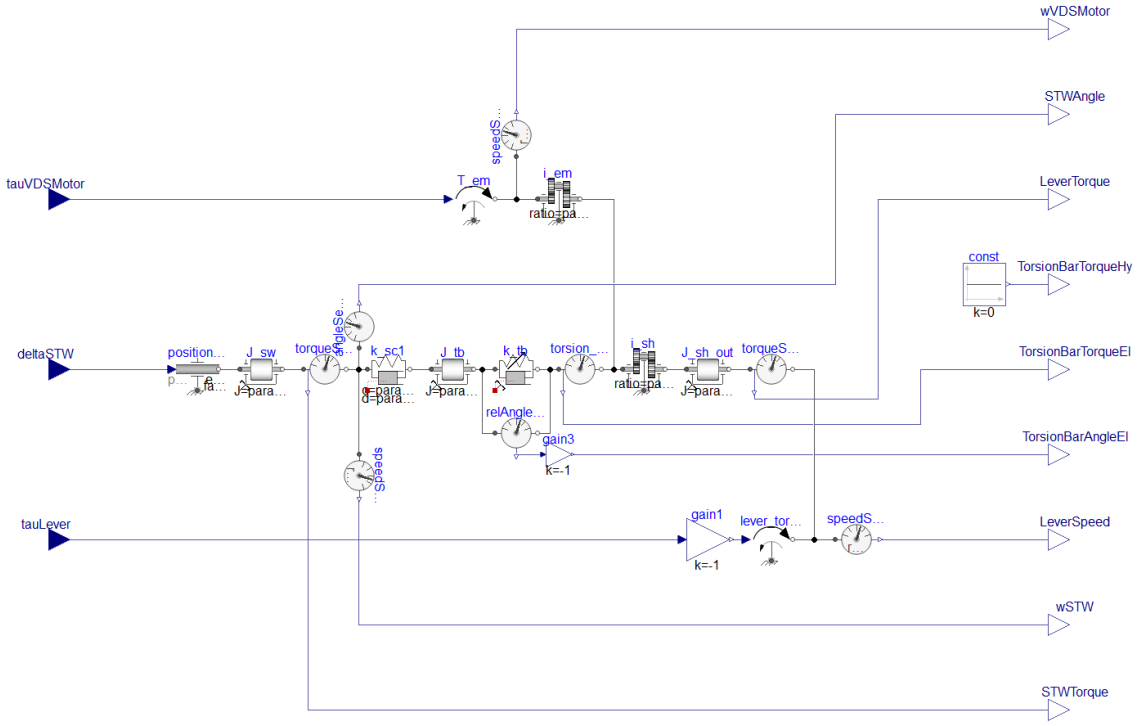

Figure 2.4: Dymola model of the EPS topology with steering wheel angle as input and pitman-arm torque as power bond.

sharing names between the two topologies also have the same parameter values. This includes k_{sc} and k_{sc1}.

Both topologies contain three inertias: The steering wheel inertia J_{sw}, the torsion bar inertia J_{tb} and the output inertia $J_{sh,out}$. The VDS-like topology also contains a piston mass inside the hydraulic gearbox called `boostCurve` in Figure 2.3. It's linked to $J_{sh,out}$ through a gear ratio but without springs in between like the other inertias have. Therefore, the piston mass can be considered part of $J_{sh,out}$ when analyzing the dynamics of the system. Each inertia provides two states for the control, an absolute angle and an angular velocity, making these topologies 6^{th} order systems when linearized. The steering column's and steering shaft's combined inertias are relatively small compared to the steering wheel's and were therefore assumed to be negligible.

The two topologies contained two springs, one for this steering column and steering shaft k_{sc} (or k_{sc1}) and one for the torsion bar and the spindle of the worm gear in the gearbox k_{tb}. See a typical gearbox in Figure 2.5 below. By lumping the springs in series according to

$$k_{eq} = \frac{1}{\frac{1}{k_1} + \frac{1}{k_2}} \tag{2.1}$$

and putting the equivalent spring constant k_{eq} in one spring block in Dymola instead of two springs coupled in series, the risk of numerical instability is decreased [15].

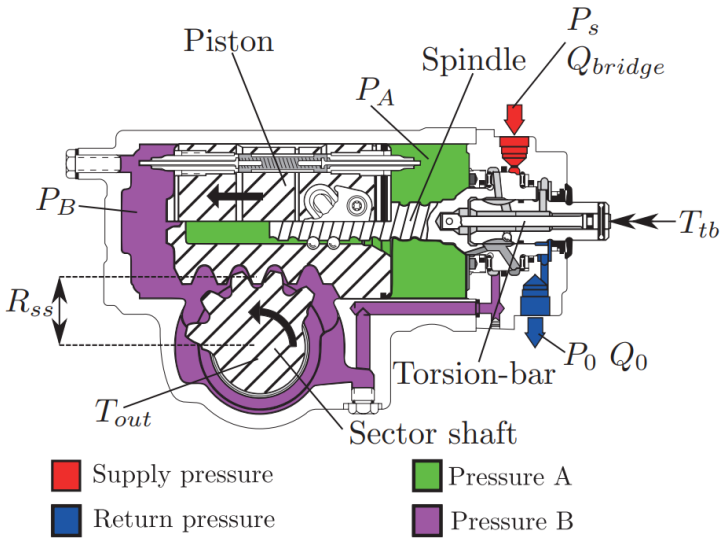

Figure 2.5: Inside of a typical steering house [14]

The steering wheel's spring was assumed to be stiff enough compared to k_{sc} to only generate small and negligible high-frequency oscillations and was therefore left out.

To the right in Figure 2.5, the limiting mechanism is vaguely depicted. It transfers torque past the torsion bar, if the torque gets too high, to protect the bar from breaking. This would introduce discontinuities to the model which would increase complexity. To avoid this but still model the change satisfactorily, the k_{tb} spring in Figure 2.3-2.4 was modeled with a linear region between an upper and lower bound $\pm\delta_{tb,0}$. Above and below these bounds, the displacement-to-torque curve becomes a third-order polynomial with the same first-order term as for the linear region but with an additional third-order term as shown in (2.2). To make the first order region transition into the third order region smoothly, the linear term $c_{lin,non}$ is multiplied with the unfiltered displacement angle $\phi_{rel,T}$ but the third order term $c_{non,3}$ is multiplied with the displacement angle but starting from zero at the transition points. By having the third-order term set to zero at the transition points, the non-linearity is introduced smoothly.

Note: To get a visual reference of what is explained above and correlate to the VDS-like model, figure 2.6 which is derived from figure 2.3 is the model of the mechanical system depicted in figure 2.5.

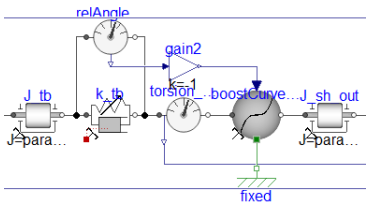

Figure 2.6: Model of the mechanical boost (zoomed in from figure 2.3)

$$\begin{cases} T_{k,tb} & = c_{lin,non} \cdot (\phi_{rel,T} - \delta_{tb,0}) + c_{non,3} \cdot (\phi_{rel,T} - \delta_{tb,0})^3 \quad \forall\ \phi_{rel,T} \notin [-\delta_{tb,0}, \delta_{tb,0}] \\ T_{k,tb} & = c_{lin} \cdot \phi_{rel,T} \quad \forall \phi_{rel,T} \in [-\delta_{tb,0}, \delta_{tb,0}] \\ c_{lin,non} & = c_{lin} \end{cases} \tag{2.2}$$

The code for the Dymola model of the non-linear torsion bar spring is shown in Appendix A including the implementation of the transitioning between regions using Modelica's `homotopy()` operator as explained in [16].

Both topologies also contain gears. One for the motor (I_{em}) and two in the gearbox. The hydraulic gearbox in Figure 2.5 shows how rotational movement of the torsion bar and spindle translates to transnational movement of the piston and then back to rotational movement of the sector shaft. But since the EPS topology doesn't have any hydraulics, the two gears were combined into one as seen in Figure 2.4. Inertia reflected over a gear is equal to the inertia divided by the square of the gear ratio [17] as follows:

$$J_{motorside} = \frac{J_{wheelside}}{I_{em}^2} \tag{2.3}$$

This makes the road wheel inertia appear smaller on the electric motor's side of the system. The same effect also makes the inertias of the steering wheel, torsion bar and the electric motor appear bigger at the road wheel side of the systems, decreasing the impact of disturbances originating at the road wheels before reaching the driver. However, it also contributes to making the $J_{sh,out}$ inertia appear bigger than J_{tb}, making J_{tb} even smaller compared to the rest of the system's inertias.

The last moving components of the topologies are modeled in the hydraulic gearbox, called `BoostCurve_Coded3`, which only is included in the VDS-like topology (Figure 2.3). Apart from the gears mentioned earlier, it contains hydraulics which adds force to the piston based on the measured deflection angle of the hydraulic torsion bar. The force needs an equal but opposite reaction. In reality, this force comes from the pressure from the hydraulic oil which in turn pushes on rigid surfaces. Therefore, the opposite reaction was modeled against a fixed wall, the green "floor" under the `BoostCurve` in Figure 2.3.

The assistance to the driver should be significantly much higher at higher torque inputs to improve the steering feel [14]. To achieve this, the toque boost follows a third-order polynomial from torsion bar deflection to added torque. As long as the torque to the torsion bar is within its linear region, it is directly proportional to the torque. However, the hydraulics have an upper bound of how much torque can be added. To limit the hydraulic torque output, the `homotopy()` function, mentioned earlier, was used again. This is described more in detail under section 2.3.4.

The hydraulic fluid also has a significant amount of dampening compared to the rest of the system and compared to the EPS topology. This can pose a difficulty when it comes to attenuating high-frequency oscillations of the torsion bar inertia in the EPS topology.

2.3.2 Sensor placements and power bonds

As seen in Figure 2.3-2.4, the Dymola models contain 8-9 sensors. Out of these, the only ones that can be assumed to be measured in reality are the steering wheel's angle, the steering wheel's angular velocity, motor position and the torsion bar torque. The angular velocity is obtained through derivation of the angle and the torsion bar torque is obtained by multiplying the bar's deflection angle with the spring constant. Therefore, these signals can also be obtained in the real world.

The pitman-arm's angular velocity is not measured in reality but is still used in the simulation environment together with the `tauLever` input to ensure conservation of power ($P = \omega \cdot T$). This is to make sure energy isn't created in parts of the system where it's not supposed to and to be able to connect the system outside the Dymola model in a physically meaningful way. The same goes for the electric motors' torque input `tauVDSMotor` and the speed sensor connected to the same node in Figure 2.3-2.4. The feedback from the external system, or the upper and lower inputs to the Dymola models will be referred to as the power bonds or p-bonds.

Since the hydraulic torsion bar works by opening and closing valves, and connecting chambers of different hydraulic pressures, it doesn't need to be electronically controlled for the hydraulics to be able to support the driver input. Therefore, it doesn't need to be measured in reality. The hydraulic torsion bar torque was however connected to an output for monitoring just like the rest of the sensors in Figure 2.3-2.4 that weren't mentioned.

The sign convention used for modelling is to have a positive direction pointing out of the steering wheel, i.e. counterclockwise (CCW). This differs from Dymola's convention, where the positive direction is out from the torque, angle or angular velocity source blocks, which corresponds to the positive direction being clockwise (CW). But by staying consistent with directions inside the Dymola model, the sign of the outputs will still be correct so the direction convention does not matter. But it should be kept in mind that the sign convention differs inside the Dymola model's compared to the IPG TruckMaker simulation setup.

2.3.3 Model exportation

The Dymola models were exported in two different ways: By being converted to Functional Mock-up Units (FMUs) and as linearizations in `.mat`-files. The FMUs as seen in figure 2.7 were exported using Dymola 2022's built-in function `translateModelFMU()` found under `DymolaCommands.SimulatorAPI.translateModelFMU()` with FMI-version 2 and FMI-type set to "csSolver" as seen in Appendix B.1. The csSolver option generates a Co-simulation FMU using Dymola solvers [18].

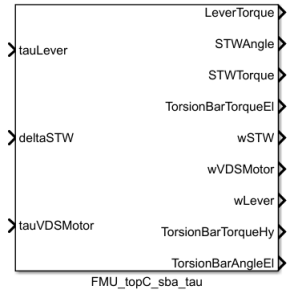

Figure 2.7: FMU export of EPS (an example)

The linearization was only done in the origin, i.e. where all inputs are zero and all states are zero. This shouldn't compromise the dynamics of the EPS model since it's a linear model. However, the VDS-like model contains the nonlinear boost curve. But for the linearization only, the boost curve in the VDS-like model was replaced with a Linear Least Squares Estimate (LLSE) of the third order polynomial connecting the torsion bar angle to the torque boost as seen in Figure 2.8. The LLSE was made of samples of the boost curve between the min and max values of the boost curves operational region described earlier. This was done in order to mitigate the error throughout the operational region of the boost curve.

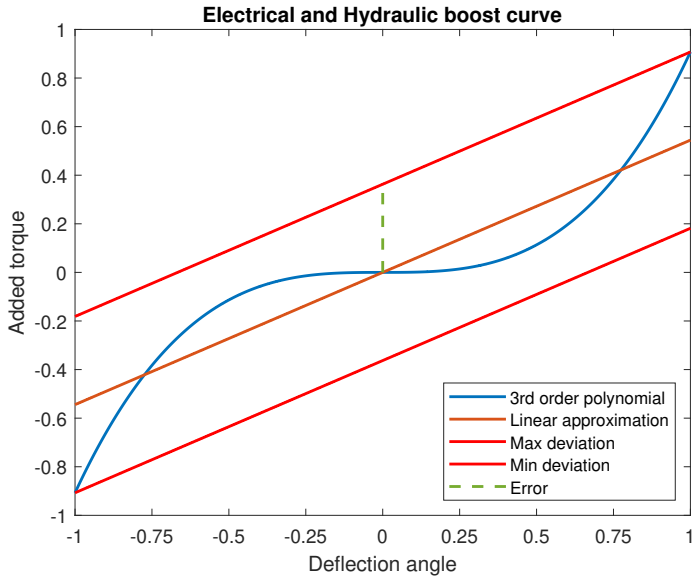

Figure 2.8: Actual hydraulic boost curve compared to its LLSE and the error difference between the two

2.3.4 Validation and verification of the Dymola model

To evaluate whether the modeled parts work as intended, test simulations were made. This includes the nonlinear torsion bar model, the nonlinear boost curve and the VDS-like topology as a whole. Since the EPS model happens to have the same number of states, and largely shares the same components as the VDS-like topology,

the evaluation of the VDS-like topology is assumed to be sufficient to validate and verify both topologies.

2.3.4.1 Custom components

The test case for the nonlinear spring was set up in Dymola according to Figure 2.9. There's a ramp input to the left, starting below the linear region's lower end point and ending at the same value but with an opposite sign. This signal was fed to an angular source block, converting the raw number into an angle. The angle source block was connected to the inertia of arbitrary size just to make the angular velocity well-posed. This was needed to get around errors. The inertia is then in turn connected to the nonlinear torsion bar model which was connected to a fixed wall. The third-order coefficient was increased from that used in the topology models to put emphasis on the linear versus nonlinear regions.

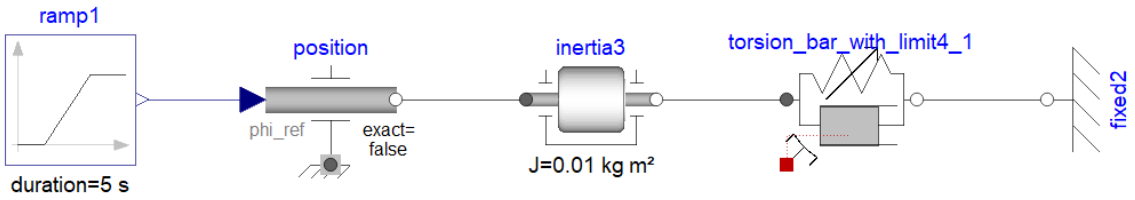

Figure 2.9: Simulation setup for verification of the nonlinear torsion bar Dymola model

The simulation results can be seen in Figure 2.10 below, confirming the torsion bar's linear region in the middle and the third-order polynomial behaviour on the outer edges. It can also be seen that the transition between linear and nonlinear regions are smooth. Finally, the torque has the opposite sign compared to the angle since the torque it is measured from `flange_b` of the torsion bar, i.e. the right connection. This follows Dymola's sign convention of action and reaction for a-flanges and b-flanges, depicted in black and white respectively.

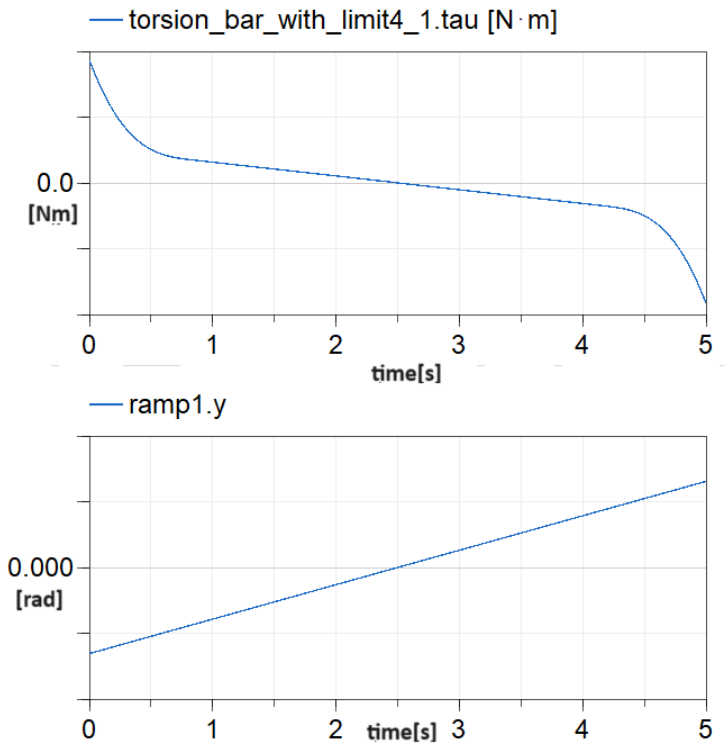

Figure 2.10: Simulation results from the model of the nonlinear torsion bar showing angular deflection in the bottom and torque in the top

The simulation setup for the hydraulic gearbox was made similar to that of the nonlinear spring and can be seen in Figure 2.11. It begins with a ramp input starting below the third order polynomial region. This is converted to a torque connected to an inertia of arbitrary size, just as before. The inertia was connected to a linear spring-damper instead of the nonlinear torsion bar model to be able to verify the curve shape of the torque boost's curve shape. Unlike in Figure 2.3, the relative angle sensor was placed upside down, giving the same effect as changing the sign with a -1 gain. The right-most inertia was added for the same reasons as described earlier.

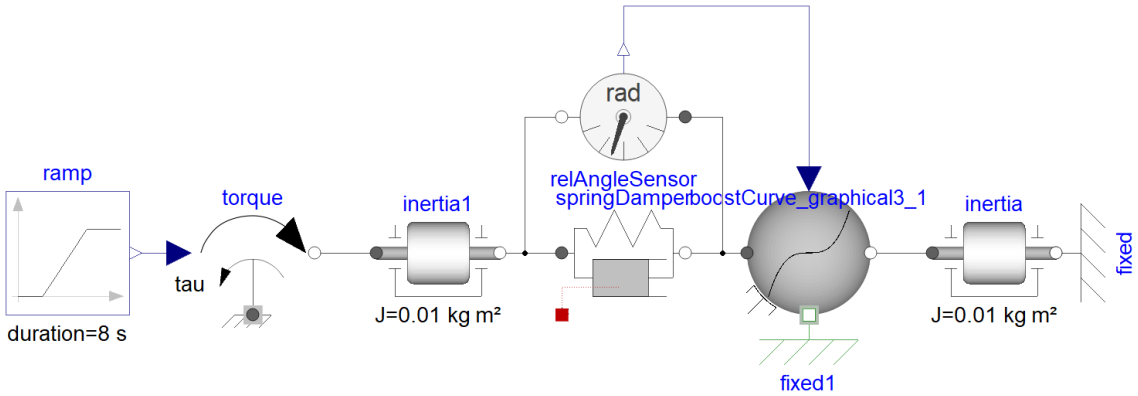

Figure 2.11: Simulation setup for verification of the hydraulic gearbox Dymola model

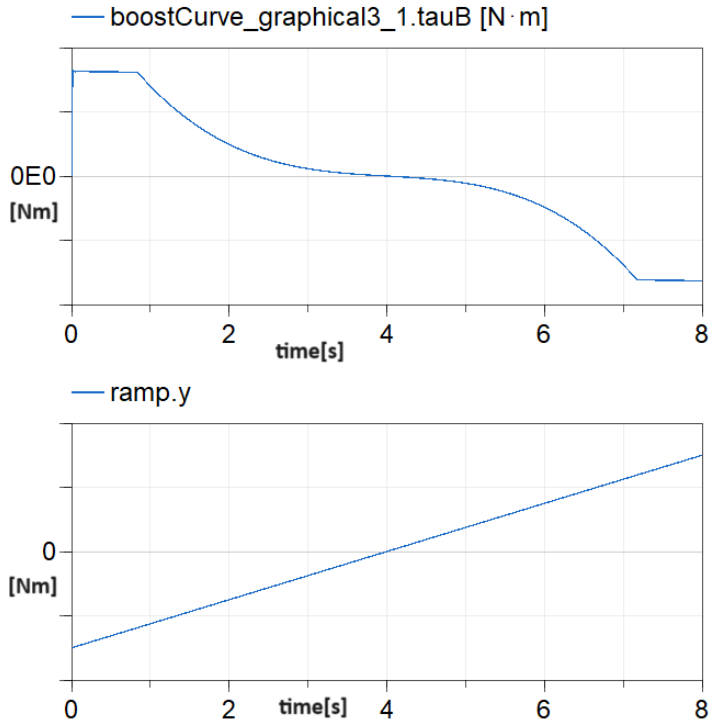

Figure 2.12: Simulation results from the model of the hydraulic gearbox, showing input torque at the bottom and the resulting torque boost at the top

The results of the simulation can be viewed in Figure 2.12 which confirms the third-order polynomial curve shape within the operational region of the hydraulics. Outside the operational region, the torque boost is kept constant at the max or minimum values. Once again, the sign difference between the input torque and the output torque is due to Dymola's action-reaction convention of the a- and b-flanges.

2.3.4.2 The Dymola model of the VDS-like topology

To check the correctness of the developed VDS-like model, a comparison is made with the provided ground truth FMU. This test setup includes an inertia load connected to the FMU as shown in figure 2.13 where `tau` is the torque output of the inertia load and `w` is the rotational velocity fed to the inertia load.

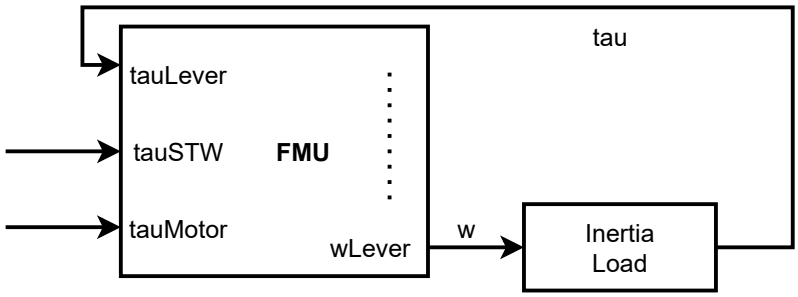

Figure 2.13: FMU with inertia load

Because the provided ground truth FMU was designed for torque-based steering, the

tested VDS-like model also employs the same steering method. The `tauMotor` input was set to zero, indicating that the motor was inactive. To evaluate and contrast the steering performance, both sine and step inputs were applied to `tauSTW`. The lever speed ω serves as the input for the inertia load, and the resulting `tau` is looped back into the FMU to maintain the power bond.

The observations from this comparison will be discussed in chapter 5.

2.4 Electric Motor for Steering

The VDS-like topology and the EPS are reliant on motors to perform various functions that assist driver with maneuvering. For VDS-like, the motor contributes to functions related to comfort and safety. Motor for EPS on the contrary has a requirement analogous to the functioning of hydraulic boost from the VDS-like topology, along with providing active safety utility.

2.4.1 Motor Requirements Considered

- **Torque Output:** The motor should be capable of producing sufficient torque to assist the driver's steering inputs, especially at low speeds when the steering effort is higher. The torque output of the motor depends on factors like the vehicle's weight, tire size, and desired steering feel.
- **Speed Range:** The motor should operate effectively over a wide speed range, from very low speeds during parking maneuvers to higher speeds during highway driving. This ensures that the power steering assistance is available across various driving conditions.
- **Control:** The motor should be controllable to provide different levels of torque assistance based on driving conditions. This requires a well-designed motor control algorithm that adjusts assistance based on parameters like vehicle speed, steering angle, and driver inputs.
- **Compact Size:** Space within the vehicle is often limited. The motor should be designed to fit within the available space without interfering with other components. Also, the motor inertia must be minimal in order to be responsive.

2.4.2 Motor Design

The motor considered for the steering operation is a Brushless Direct Current (BLDC) motor [19]. This is specifically because:

- **High Power Density:** BLDC motors typically have a higher power-to-weight ratio, perfectly suiting the steering requirement as space and weight are critical factors.
- **Smooth Operation:** The electronic commutation in BLDC motors provides smoother and more precise control over speed and torque, resulting in

smoother motion profiles and better overall performance.

- **Torque Control:** BLDC motors offer precise torque control through techniques like current control. These control methods enable the motor to maintain a desired torque output even under varying loads and speeds.
- **Dynamic Response:** BLDC motors can provide rapid changes in torque output due to their low inertia and efficient control strategies. This responsiveness is crucial as steering demands quick changes in speed or load.

Since the two different steering topologies have different functional requirements, two different motors are selected whose parameters are found in tables-C.1 and C.2 found in appendix. It should be noted that 3 Nm and 10 Nm motors are used for the VDS-like and EPS topologies respectively.

These motors were modeled in Simulink using the default block `Permanent Magnet Synchronous Machine` as seen in figure 2.14 and then changed to BLDC in the settings.
The IOs seen in figure 2.14 are the phase voltages `A, B, C`, rotor speed `w` and a vector of outputs `m` that include speed, torque, stator currents, back EMF, etc.

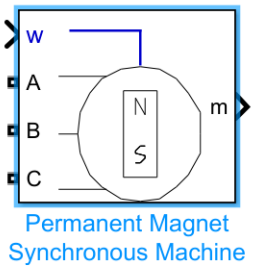

Figure 2.14: Default motor block from Simulink

Since BLDC motors work on electronic commutation, a dedicated current controller that generates the gate pulses that operate the power electronic converters to meet the load request is required for its operation. This is discussed in detail in the Controls chapter.

3
Control

3.1 Introduction

The only controlled input to the two topologies is the motor torque. To control the motor, two control loops were implemented. The innermost controller will, from here on be referred to as the motor control or the PI controller. And the outer will be referred to as the outer controller or the $\mathcal{H}_2$ controller.

The reason for using an $\mathcal{H}_2$ controller is because it is energy optimal [20]. More specifically, it aims to minimize the $\mathcal{H}_2$ norm of the transfer function of the closed loop system, including the plant and controller, from the exogenous inputs n, d, and r to the performance outputs z_2 depicted in Figure 3.1. This makes the $\mathcal{H}_2$ norm the cost function of the optimization problem. Note that the performance outputs may contain more signals than the measured ones (v). With a small $\mathcal{H}_2$ norm, the performance outputs become smaller for a given set of exogenous inputs.

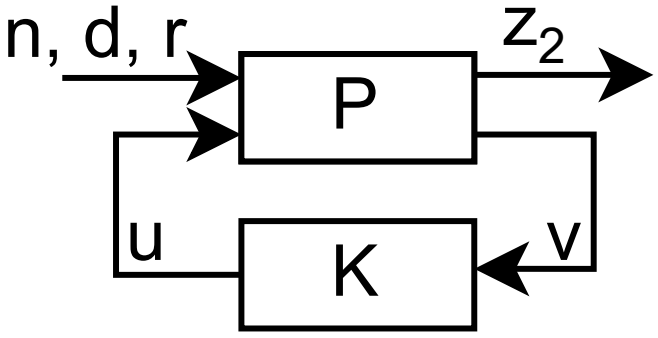

Figure 3.1: The PK-structure where P includes the Dymola model and signal weights, K is the controller, n is the noise, d is the disturbance, r is the reference signal, u is the control signal, v is the signals of the measured outputs and z_2 is the performance outputs.

The $\mathcal{H}_2$ norm is defined according to (3.1). This means the cost function is quadratic in the states. If the states are velocities or angular velocities, the minimization of the $\mathcal{H}_2$ norm, which is equivalent to minimizing the energy of the impulse response of the closed-loop system [20], will also minimize real-world energy. By having

an energy-optimal controller, less energy is needed for steering and therefore more energy can go to propulsion, increasing the driving range of the vehicle.

$$\|T\|_2 = \left(\frac{1}{2\pi}\,\mathrm{Tr}\left[\int_{-\infty}^{\infty} T(j\omega)^* T(j\omega)\right] d\omega\right)^{1/2} \tag{3.1}$$

The high-level control strategy can be seen in Figure 3.2. The main component is the plant, i.e. the linearized Dymola model mentioned in section 2.3.3, connected to a boost curve and the motor. The electrical boost curve was only applied for the EPS model and the motor block is different for the two different topologies as mentioned before. The two exogenous inputs `stw input`, i.e. the driver imposed steering wheel angle, and the `p-bond input`, i.e. the lever torque, are both disturbances perturbing the performance outputs of the $\mathcal{H}_2$ norm. The u_b is the control signal resulting from the electric torsion bar torque's deflection angle $\delta_{tb,e}$ being passed through the third order boost curve depicted as `boost`. u_b is then added to the main outer control loop's control signal u_{outer} to form u_m. u_m is the control signal passed onto the inner control loop in the motor block.

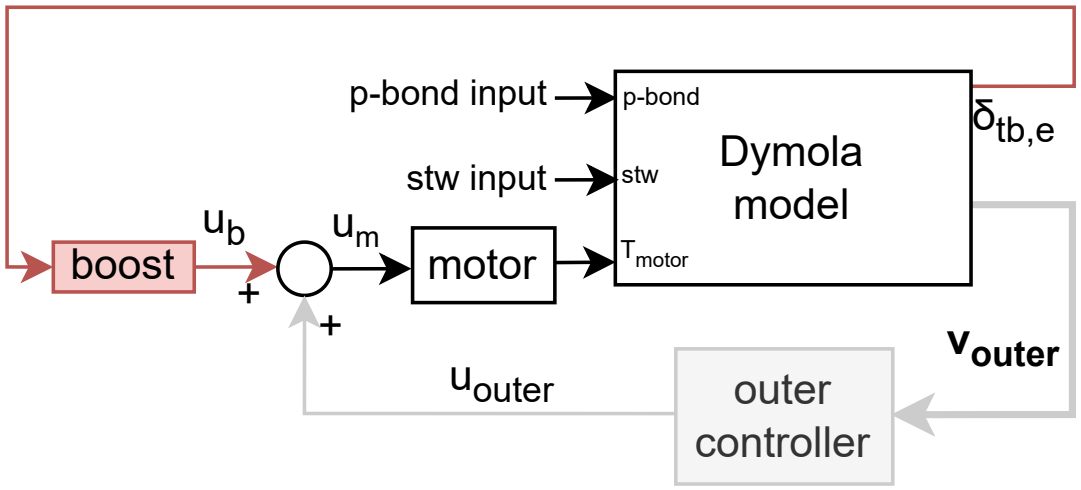

Figure 3.2: High-level control strategy containing a boost curve for the electrical motor, the electrical motor, the outer controller, and a linearization of either Dymola model. The motor and Dymola model differs between EPS and EHPS. The boost curve-related block and signals depicted in red are only included for the EPS model and left out for the EHPS model.

3.2 Controller Synthesis

The block diagram for the $\mathcal{H}_2$ control synthesis is depicted in Figure 3.3. It is almost identical to the high-level control block diagram in Figure 3.2 except for the weighting functions W_p, W_{stw}, W_{inf} and W_2.

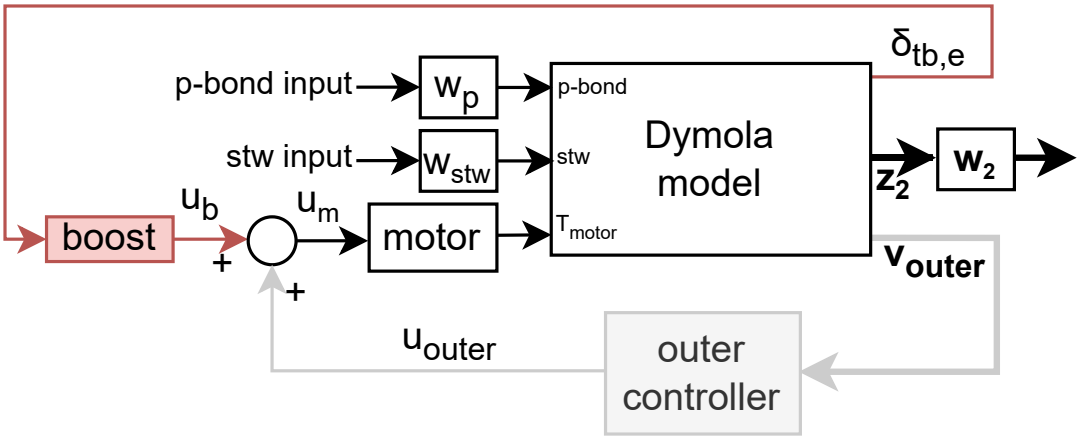

Figure 3.3: Block diagram used for the $\mathcal{H}_2$ controller synthesis.

3.2.1 Weightings

With $\mathcal{H}_2$ controllers, the inputs and outputs (IOs) are assumed to be of unit size. However, the simulation results in Chapter 5 show that all signals have other magnitudes. Therefore, the weights were added, scaling the complete model's IOs such that the IOs of the Dymola model had correct magnitudes.

$\mathcal{H}_2$ control synthesis also assumes the frequency contents of the complete model's IOs to be uniform as procuring these frequency contents posed to be a challenge. Two methods were employed to determine the frequency content which were the `Control System Designer App` of simulink and `Fast Fourier Transform` (fft) method. These methods were however futile as the former method requires complete access and control of the simulink workspace to perform the bode analysis. Since the model is within the truckmaker for simulink environment, the designer app is restricted from obtaining the control of truckmaker for simulink environment. The latter method involved using the `fft` to obtain the bode plots where the appropriate input and output signals were recorded. Though a bode plot was obtained, it demanded significant post-processing.

As a work-around to obtain just the weights, the test runs from both driving scenarios which are driving in figure 8 and wheel lock were considered. All the IO signals associated to the FMU were recorded for the two different runs. It was observed that the peak values of these signals obtained from the wheel lock scenario was maximum as opposed to figure 8 driving. Hence, following the procedure for controller synthesis, the weights were selected to be reciprocal of these peak values that can be seen in the appendix as table D.1.

3.2.2 Electric boost

As explained earlier, the third-order polynomial boost curve of the EHPS system is implemented through hydraulics and aims to improve the steering feel. To achieve a similar steering feel with the EPS system, a boost curve was added to the control law

as seen in Figure 3.3. Just as for the hydraulic boost, the electric boost depends on the deflection of the torsion bar modeled just before the added torque's connection to the main shaft running through the middle of Figure 3.4.

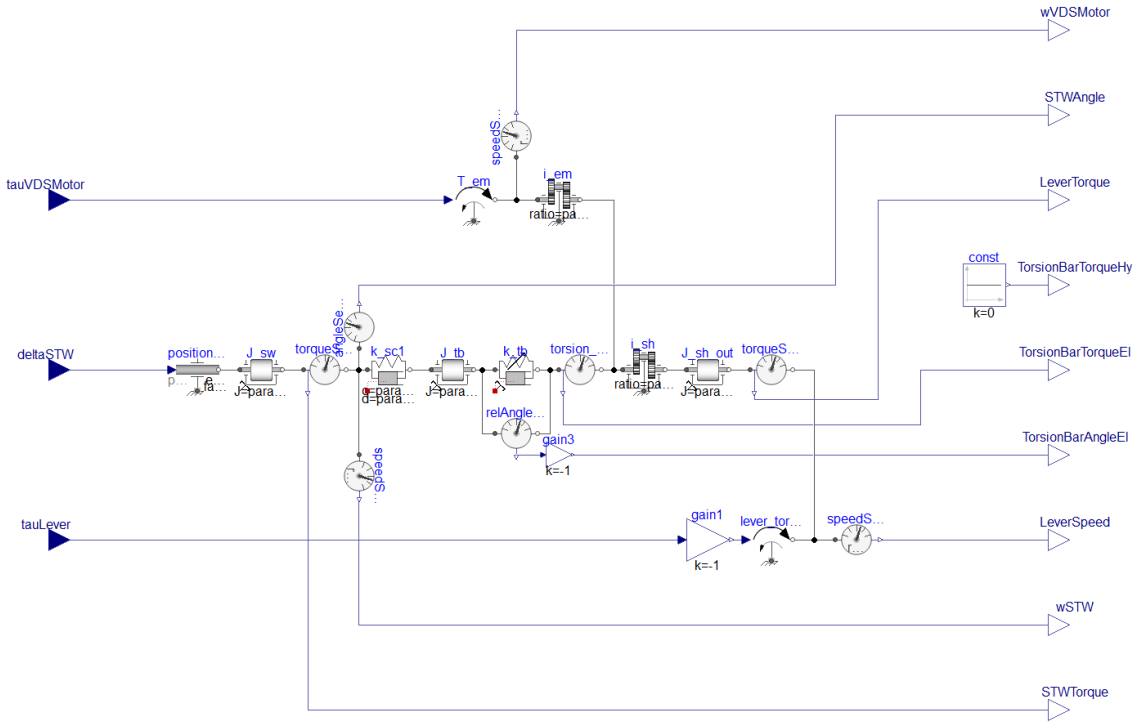

Figure 3.4: Dymola model of the EPS topology with steering wheel angle as input and pitman-arm torque as power bond (Figure 2.4 repeated for convenience).

To make the two topologies comparable, the electric boost hydraulic one should achieve the same amount of torque at the road wheels and the steering wheel for a given torsion bar deflection angle. To achieve this, the parameters of the third-order polynomial describing the added torque given a deflection angle of the hydraulic torsion bar were used. But the added torque from the electric motor is amplified through a different set of gear ratios compared to the hydraulic one as shown in Figure 3.4. Therefore, the electric boost curve was obtained by dividing the third-order polynomial hydraulic boost curve by the worm gear ratio and the electric motor's gear ratio as following:

$$\begin{aligned} B_e &= \frac{B_h}{i_{wr} i_{em}} \\ &= \frac{\gamma_{h,1}}{i_{wr} i_{em}} \delta_{tb} + \frac{\gamma_{h,2}}{i_{wr} i_{em}} \delta_{tb}^2 + \frac{\gamma_{h,3}}{i_{wr} i_{em}} \delta_{tb}^3 \\ &= \gamma_{e,1} \delta_{tb} + \gamma_{e,2} \delta_{tb} + \gamma_{e,3} \delta_{tb} \end{aligned}$$

Note that the subscript of the torsion bar deflection angle δ_{tb} doesn't specify if it's the electric or hydraulic one. This is because the stiffness of the two torsion bars are approximately the same, making them deflect approximately the same for a given torque. Therefore, the boost added for a given torque should be about the same in the two topologies.

3.3 Electric Motor Operation and Control

3.3.1 Motor Control Setup and Theory

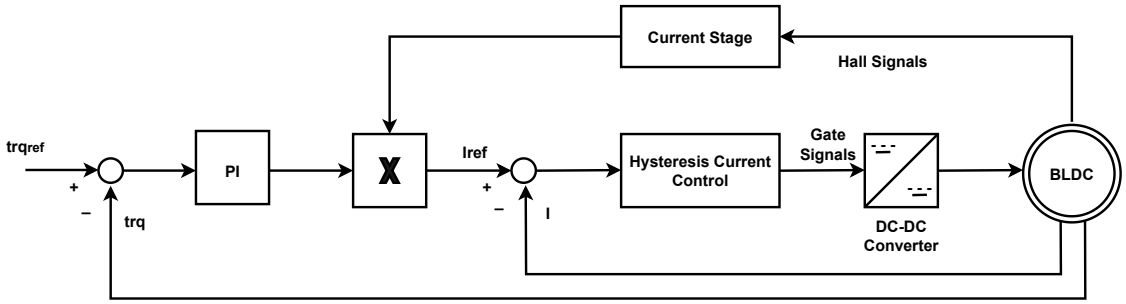

Figure 3.5: Motor Control Block Diagram

In a closed-loop torque control drive as seen in figure 3.5, the instantaneous motor torque is utilized as feedback, which coupled to an appropriate control system, results in the torque control of the motor[21].

The outermost controller provides the appropriate torque as reference which meets the driving maneuver. The difference between the reference torque and the measured actual torque results in an error signal. This error signal multiplied with the motor torque constant results in a reference current. This reference current is subsequently compared against the real stator currents, and the resulting error is fed into the hysteresis current controller. The hysteresis current controller generates gating pulses that regulate the activation or deactivation of power electronic switches in the DC-DC converter. Through precise switching operations, this converter is manipulated to govern the stator currents powering the BLDC motor.

3.3.2 Simulink Implementation of Motor Control

Since the requirement in this thesis is limited to a motor delivering torque as demanded by the assist to support the driver, a simple control topology is implemented without considerable focus on converter performance, torque ripple reduction, position measurement using hall sensors and motor efficiency. Control of BLDC is reliant on robust digital control of power electronics within the converter. With a basic converter as used here, this compromise in performance is expected.

Figure 3.6 depicts the utilization of MATLAB Simscape for the Simulink implementation. The BLDC motor is designed as discussed in section 2.4. The Hall sensor signals are used in the decoder block to obtain the three-phase stator currents I_{abc} state which could be `+DC`, `-DC` or `0` (tables 3 and 4 in [19]).

Gate signals that control the DC-DC converter are generated by the Hysteresis Current Controller. This indirect method of torque control involves the conversion

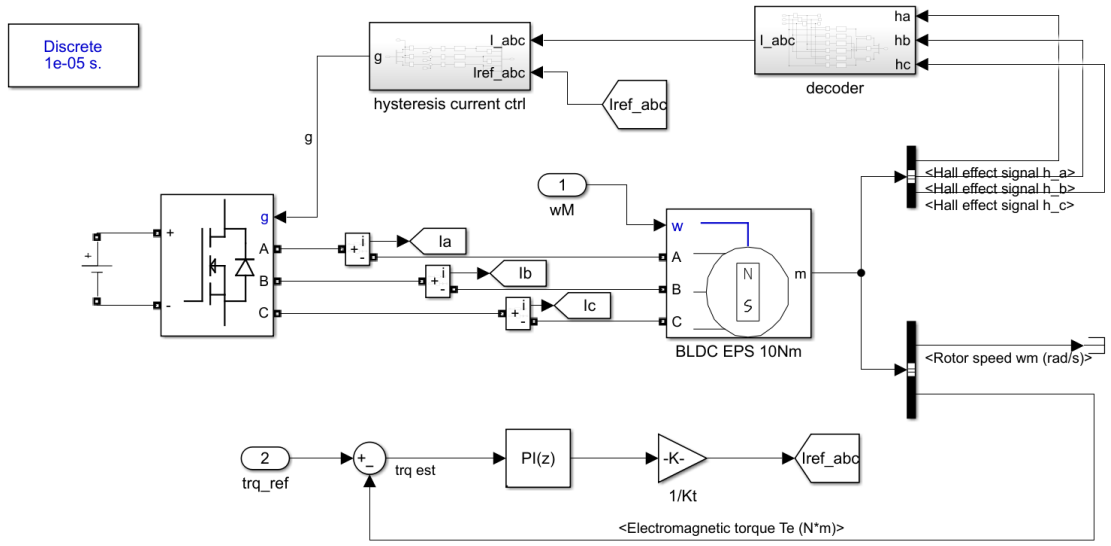

Figure 3.6: Simulink Implementation of Motor Control

of torque to current considering the motor torque constant which is seen as $Iref_{abc}$ in figure 3.6. The reference current signal is first generated by the controller by obtaining the product of $Iref_{abc}$ and I_{abc} as seen in the figure above. The actual stator currents I_a, I_b and I_c are then subtracted to procure the error in current. This error is then passed through a `Relay` block which outputs in binary. These binary signals constitute the gate pulses (tables 3 and 4 in [19]) that fire the power electronic switches (power MOSFETs) hence closing the loop.

The PI controller implemented here was tuned by trial and error which possesses the controller constant values of k_p and k_i as 11 and 0.8 respectively.

The FMU supplies the motor model with the speed of the rotor shaft, which serves as an input. This speed represents the operational speed of the motor. With the motor getting the speed reference from the FMU and the motor supplying the torque to the FMU, a power bond is established.

3.3.3 Motor Control - Results

Validation of the motor model was done by providing a torque reference signal that resembles moving the steering wheel left and then right while delivering a certain torque. As a speed signal input, a signal that resembles the torque signal contours was also connected.

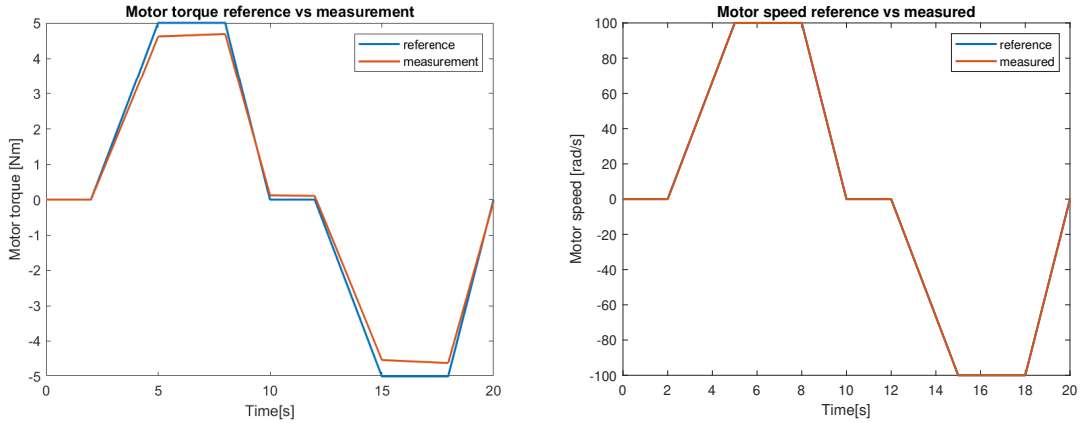

(a) Motor torque - reference vs real **(b)** Motor Speed

Figure 3.7: Motor testing

From figure 3.7 it can be seen that the motor follows the reference. There is however a small error when attaining the maximum torque.

3.3.4 Simplified electric motor

For a controller to perform well and counter the system dynamics, all the elements that constitute the plant model must be included during the controller synthesis stage. The motor having been developed in the simulink environment and not in dymola, it was imperative to include the motor model at the time of controller synthesis.
A simple first-order low-pass filter was deemed to be a sufficient approximation of the motor. The filter equation can be seen in equation 3.2 where ω_c is the cut-off frequency.

$$H(s) = \frac{1}{1 + s/\omega_c} \tag{3.2}$$

To obtain the cut-off frequency of both the motors, a chirp signal was connected as torque reference input and the output torque was recorded. The `Control System Designer App` of Matlab was used to obtain the bode plot of this data. Hence, knowing the cut-off frequencies which were 157 000 rad/s and 1550 rad/s for the 3 Nm and 10 Nm motors respectively, the low pass filter was designed and substituted.

4

IPG TruckMaker

4.1 About IPG Truckmaker

IPG TruckMaker is a specialist simulation software that provides an environment for designing, developing, and testing heavy-duty commercial vehicles. Being a high-fidelity platform, it is extensively used to accurately model both the vehicle and the test scenarios.
IPG TruckMaker provides an advanced and real-time capable vehicle model that allows users to create virtual prototypes where users can opt to substitute components with their own models. This virtual prototype can be integrated with a custom driver model, and a detailed road and scenario, enabling ample testing.
IPG TruckMaker's integration into existing tool chains is made effortless by its abundant standard interfaces and support for standard formats like FMI. Additionally, with its extensive set of interfaces, including Matlab, IPG TruckMaker can serve as a central integration platform.

4.2 Steering System

IPG TruckMaker's default steering model is discussed in this section.

IPG TruckMaker provides four different steering topologies, namely `Static Steer Ratio`, `Dynamic Steer Ratio`, `Pfeffer with Power Steering` and `Truck Power Steering`. In this thesis, none of the default steering topologies are used but the steering FMU that was discussed earlier was utilized by selecting the setting `Model Manager Off`. However, `Truck Power Steering` is presented to understand the default truck steering system design that IPG provides.

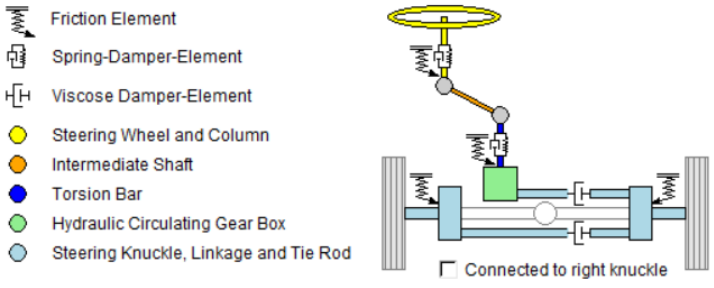

Figure 4.1: Truck Power Steering - TM default (from TM GUI)

From figure 4.1, it can be seen that the Truck Power Steering System comprises the standard steering column, intermediate shaft, and torsion bar. The torsion bar transmits motion to the circulating gearbox, causing the pitman arm to rotate at a specified ratio. Subsequently, the pitman arm facilitates the movement of the right and left steering knuckles by moving the steering linkage and drag link, respectively. A key observation here is the assumption that pitman arm is in direct connection to the steering knuckle through a linkage.

4.3 Interfacing

4.3.1 IPG TruckMaker for Simulink

TruckMaker for Simulink (TM4SL) seamlessly incorporates IPG's vehicle dynamics simulation software, TruckMaker, into the modelling and simulation environment of Matlab/Simulink by leveraging S-Function implementation and utilizing the API functions offered by Matlab/Simulink. This integration brings the highly optimized and robust features of TruckMaker into the Simulink environment. With this setup in place, the development of custom models, their integration and testing can be performed in Simulink.

To establish the link between Simulink and IPG TruckMaker's GUI and input files, the signal and variable flow between different IPG TruckMaker blocks and the signals associated with the steering system need to be understood.

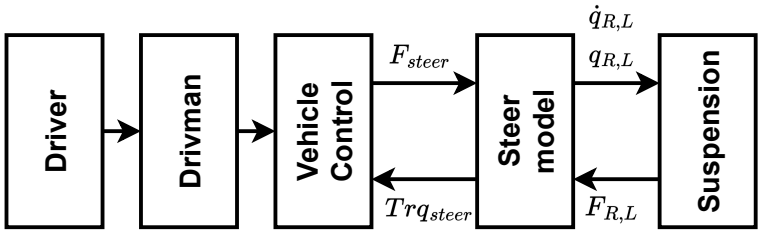

Figure 4.2: Signal and variable flow within IPG TruckMaker

Figure 4.2 shows the different blocks within IPG TruckMaker which comprise of blocks for `Driver, Vehicle Control, Vehicle Model (Steering in this case)` and `Suspension.`
The steering system is designed in a manner such that the system has a dual interface. One part is intended for the driver module, which simulates human interactions with the vehicle using blocks like `Driver` and `DrivMan.` In the presence of driver assist systems, the `Vehicle Control` module serves as the interface between the driver and the steering system. These physical variables can be seen in figure 4.2 as F_{steer} and Trq_{steer} which are Force and Torque needed to steer, respectively. The other section that interfaces with the vehicle's suspension module and as seen in figure 4.2 are $q_{R,L}$ $\dot{q}_{R,L}$ and $F_{R,L}$. Hence, the physical variables interacting with the suspension block are the steering knuckle angle and angular velocity, and forces from suspension respectively.

The steering system in IPG TruckMaker is designed to either have steer by angle or steer by torque as input. To elucidate the interaction between `Vehicle Control` and the `Steering` blocks, assume steer by angle as the type of steering. The signal exchange between `Vehicle Control` and the `Steering` blocks will then be F_{steer} and Trq_{steer} where the former is the input to the `Steering` block and the latter is the input to `Vehicle Control` block. The inputs are converse in the case of steer by torque steering setting.
As presented earlier in the report, FMUs for both these types of input have been designed. Apart from these inputs, there are a few other signals (both input and output) required for the smooth integration of FMU and the custom steering model in general to IPG TruckMaker. [22].

Inputs	**Unit**
Steering wheel angle	rad
Steering wheel rotational velocity	rad/s
Steering wheel rotational acceleration	rad/s^2
Steering wheel torque	Nm
Suspension forces	N

Table 4.1: Input signals and variables to the steering model for interfacing

Outputs	**Unit**
Steering wheel angle	rad
Steering wheel rotational velocity	rad/s
Steering wheel rotational acceleration	rad/s^2
Steering wheel torque	Nm
Steering knuckle angle	rad
Steering knuckle rotational velocity	rad/s
Steering knuckle rotational acceleration	rad/s^2

Table 4.2: Output signals and variables from the steering model for interfacing

4.3.2 Mechanical System

As discussed earlier, the default model in IPG TruckMaker has a direct link from pitman arm to steering arm. To have a relevant high-fidelity model, the dynamics of draglink is added to the model. Also added are the forces acting on the steering axle from the suspension.
Figure 4.3 depicts the steering system from the gearbox downwards up to the steering knuckle. In order to model the links between pitman arm and steering knuckle which also includes the draglink in Simulink, the following equation is considered.

$$\ddot{\delta}_{kn} = \Big(F_R + F_L + F_{buff} - \Big((\omega_{kn} - L_{pa}\omega_{pa})D_{dl} + (\delta_{kn} - L_{pa}\delta_{pa})K_{dl}\Big)\Big)/m_{axle} \quad (4.1)$$

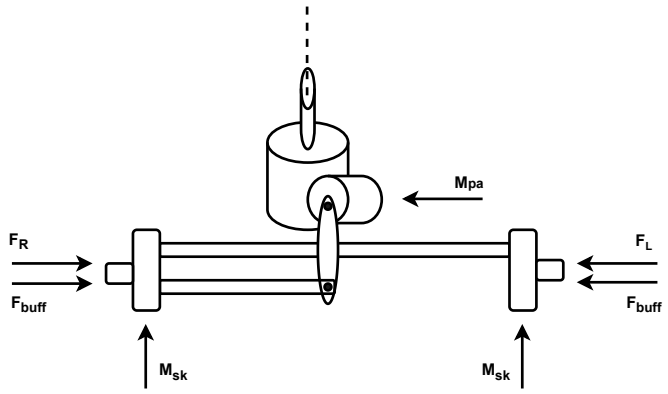

Figure 4.3: Representative figure of forces acting on steering axle. [23]

where,

F_R, F_L	forces on suspension
L_{pa}	length of pitman arm
F_{buff}	force that acts when wheel angle has reached maximum wheel turn position
D_{dl}	draglink damping constant
K_{dl}	spring constant of draglink
ω_{kn}	angular velocity of knuckle
ω_{pa}	angular velocity of pitman arm
$\ddot{\delta}_{kn}$	angular acceleration of knuckle
δ_{kn}	knuckle angle
δ_{pa}	pitman arm angle
M_{pa}	pitman arm torque
M_{sk}	torque acting at steering knuckle
m_{axle}	mass of axle

As observed in the preceding section, it is crucial for the steering FMU to generate the output that serves as the input for the steering knuckle. Therefore, based on equation-4.1, the knuckle acceleration can be computed, enabling the evaluation of both knuckle velocity and angle. Consequently, this precise evaluation establishes a seamless connection to the TM4SL interface.

Integrating the draglink with the rest of the steering linkages resulted in oscillations. The frequency content of these oscillations was utilized to calculate the D_{dl} and K_{dl} values using equation 4.2 where ζ is the damping coefficient and ω_n is the oscillation frequency.

$$\begin{aligned} K_{dl}/m_{axle} &= \omega_n^2 \\ D_{dl}/m_{axle} &= 2\zeta\omega_n \end{aligned} \tag{4.2}$$

4.4 Creating Testing Scenarios

In order to test the steering systems, a couple of test scenarios are designed in IPG TruckMaker. These make use of the default track and features available in IPG TruckMaker as seen in figure 4.4 or a custom track as seen in figure 4.5.

4.4.1 Figure-8 driving

This track as seen in figure 4.4 is specifically used to test the steering ability and power assist in making gentle left and right turns.

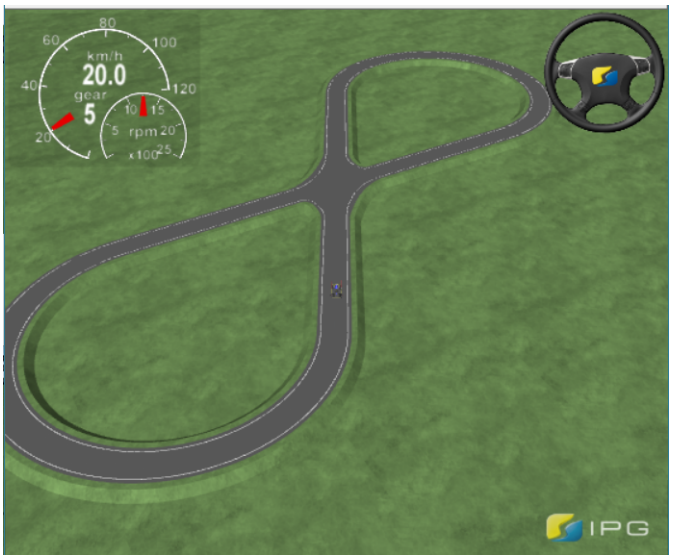

Figure 4.4: Figure-8 track

4.4.2 Wheel Lock

The wheel lock is simulated by locking either of the front wheels with the vehicle speed being a constant 40 km/h at the instance of wheel lock (at time t = 3 seconds). The initialization of this scenario is seen in figure 4.5.

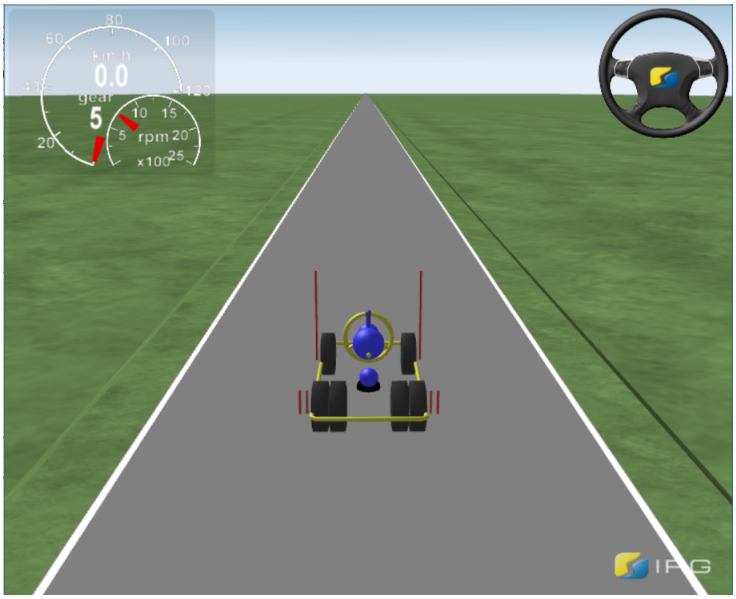

Figure 4.5: Wheel lock track

5
Results

This chapter presents all the relevant observations made during the thesis that both specifically answer the objectives as stated earlier as well as findings beyond the stated objective.

5.1 Validation of developed FMU

The ground truth FMU and the developed EHPS-FMU were both subjected to testing with an inertia load, as previously described. It is important to note that while the FMUs employed in the two driving scenarios are of the steer-by-angle type, the FMUs examined during the inertia load tests were of the steer-by-torque type. However, this distinction in types does not impact the credibility of the developed models. An acceptable steer-by-torque model automatically suggests an acceptable steer-by-angle model.
Moreover, because the EPS model was constructed based on the VDS-like model and there is no readily available EPS model for comparison, similar to the ground truth FMU for the VDS-like model, we assume that the EPS model developed in this thesis is equally accurate to the VDS-like model.

Figures 5.1 and 5.2 present the comparison of ground truth FMU with the developed VDS-like model . It is important to keep in mind that the ground truth FMU is highly realistic as opposed to the developed FMU which is based on multiple assumptions and simplifications. These plots confirm that the developed model largely behaves similarly in trend to the ground truth FMU in multiple parameters.

Steering wheel torque and lever torque are two parameters that need specific mention here. These two parameters which are outputs from the FMU, deliver lesser torque than the ground truth FMU. This behaviour could be because of the assumed inertia of certain components within the steering column and the approximation of the hydraulic boost.

5.1.1 Sine input

A `sine` block is connected to `tauSTW` which is one of the inputs as seen in figure 2.13 and this acts as a reference. The plots seen in figure 5.1 are the outputs of the FMUs.

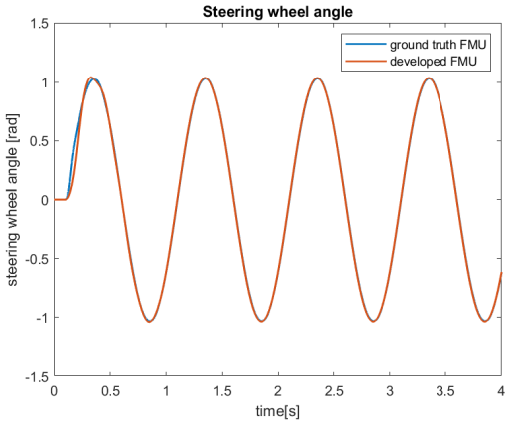

(a) Steering wheel angle

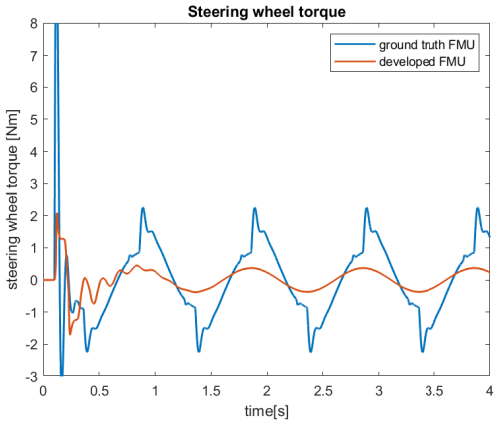

(b) Steering wheel torque

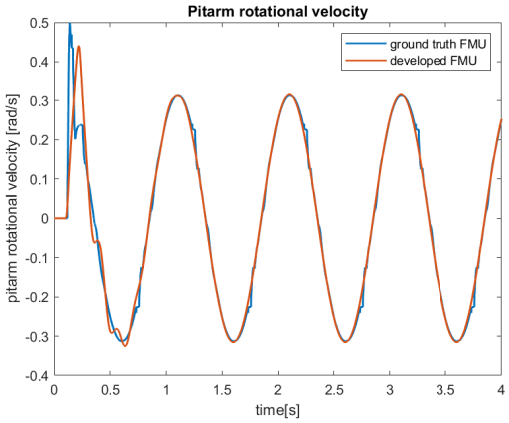

(c) Pitman arm rotational velocity

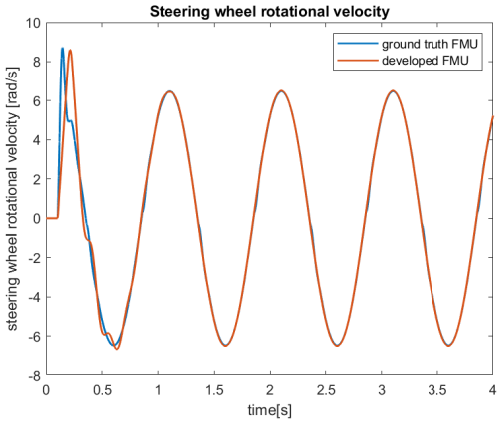

(d) Steering wheel rotational velocity

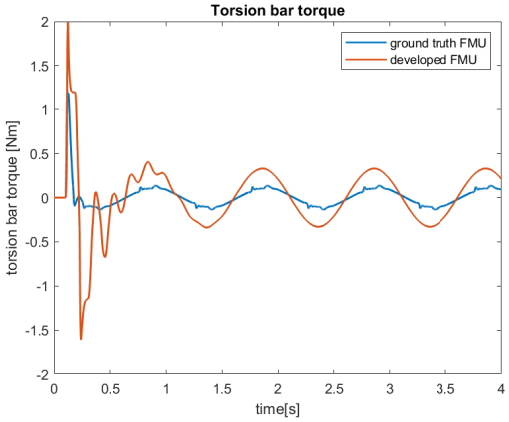

(e) Torsionbar torque

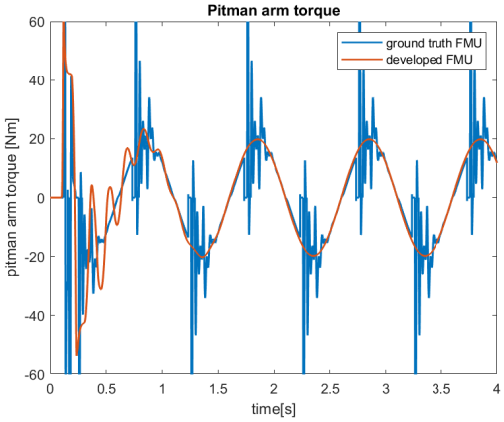

(f) Pitman arm torque

Figure 5.1: Comparison of ground truth FMU with developed steering having sine input

5.1.2 Step input

A `step` block is connected to `tauSTW` which is one of the inputs as seen in figure 2.13 and this acts as a reference. The plots seen in figure 5.2 are the outputs of the FMUs.

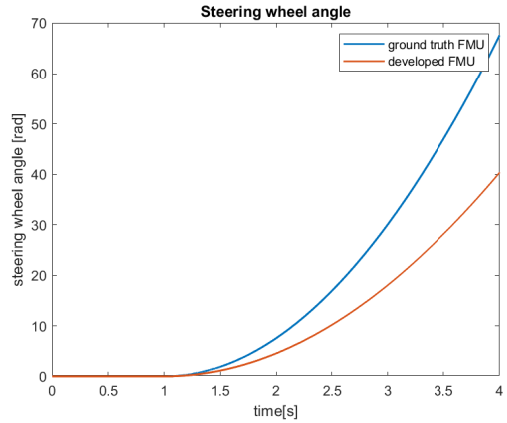

(a) Steering wheel angle

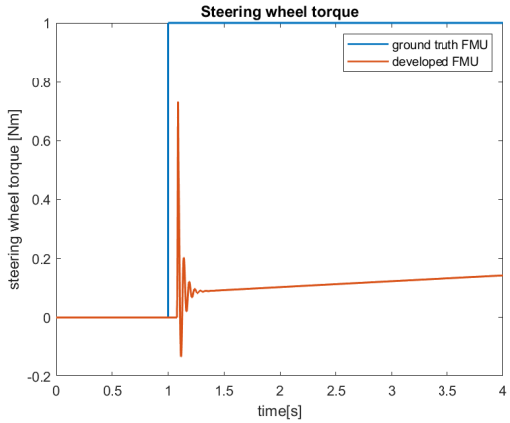

(b) Steering wheel torque

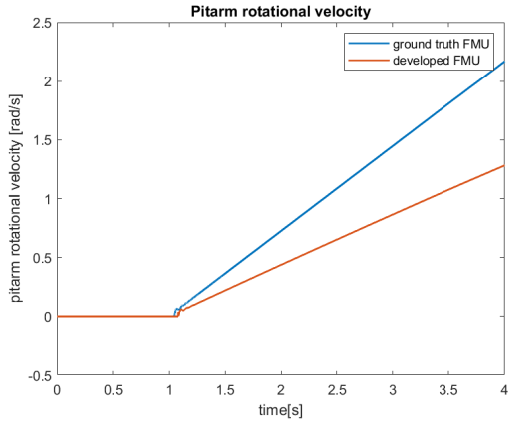

(c) Pitman arm rotational velocity

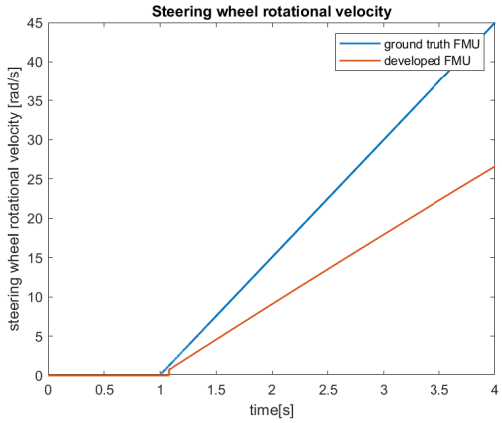

(d) Steering wheel rotational velocity

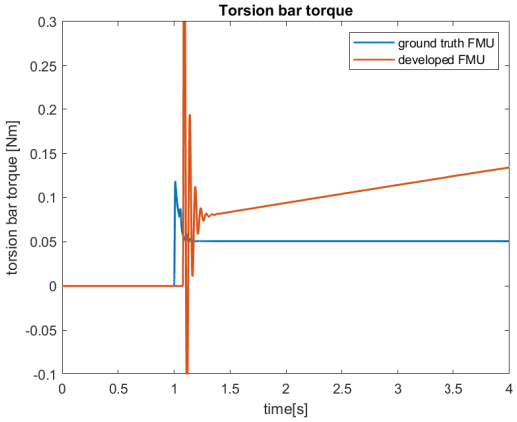

(e) Torsionbar torque

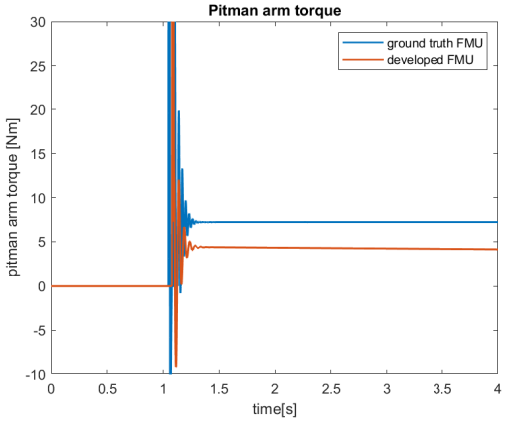

(f) Pitman arm torque

Figure 5.2: Comparison of ground truth FMU with developed steering having step input

5.2 Performance Analysis in Vehicle

The two different steering topologies were tested on the same tracks, under the same conditions. The models were tested first as an open loop system with controller (and

boost for EPS) disabled. For the EPS models additionally, just the contribution of boost without the controller was tested. Lastly, the controller (and boost for EPS) was enabled to perform the test.
A point to note here is that since EPS topology has both boost and a controller, apart from open-loop, it is tested with just boost enabled first followed by both boost and controller enabled. This way, the contribution of each entity can be observed.

5.2.1 Performance without the controller

Here, the driver makes the whole steering effort. This setup can be treated as an open-loop test where `Steering Controller` as seen in figure 1.6 is disabled. For the EPS topology however, the boost is also considered as explained later.

5.2.1.1 EHPS on figure 8 track

In this trial, the steering is controlled entirely by the driver's effort with torque assist from the motor disabled. Very small torques are needed for the driving maneuver as the hydraulic steering gearbox provides all the necessary torque for driving.

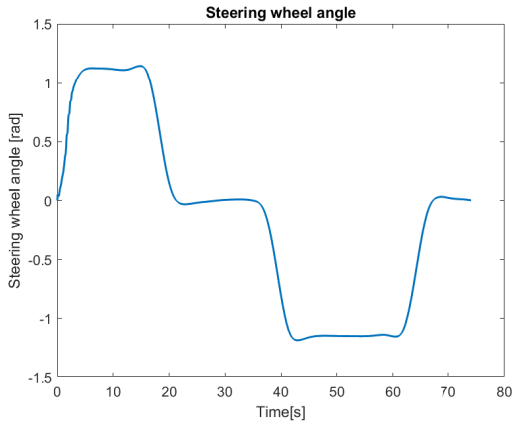

(a) Steering wheel angle

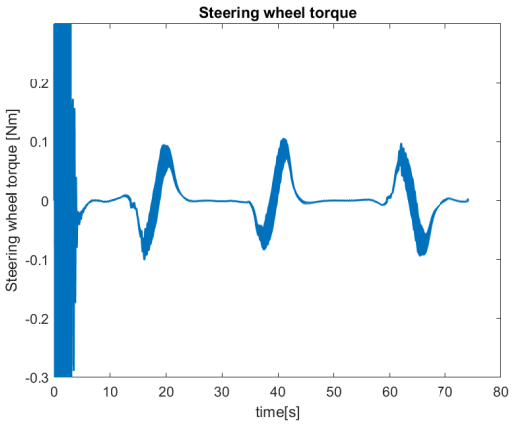

(b) Steering wheel torque

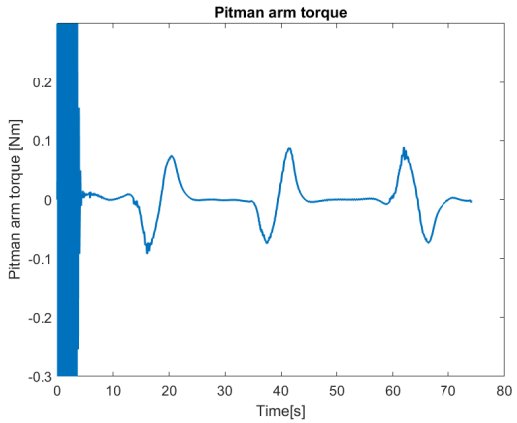

(c) Pitman arm torque

Figure 5.3: EHPS on figure 8 track

Disclaimer: The initial 3-4 seconds should not be considered as credible; they are due to some modelling/simulation instability and should not be seen as reflecting the real vehicle.

5.2.1.2 EHPS with wheel lock

Similar to the previous trial, the driver is responsible for the driving maneuver. At the time of wheel lock, when high torques are induced on the pitman arm, driver needs to put in greater effort (torque > 4Nm) to counter the situation.

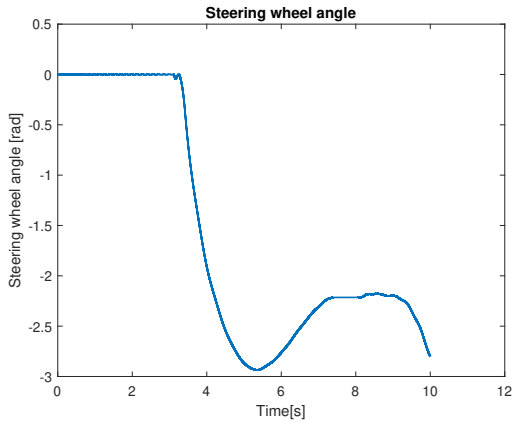

(a) Steering wheel angle

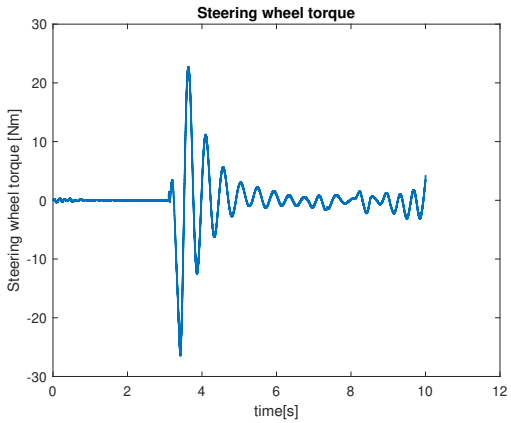

(b) Steering wheel torque

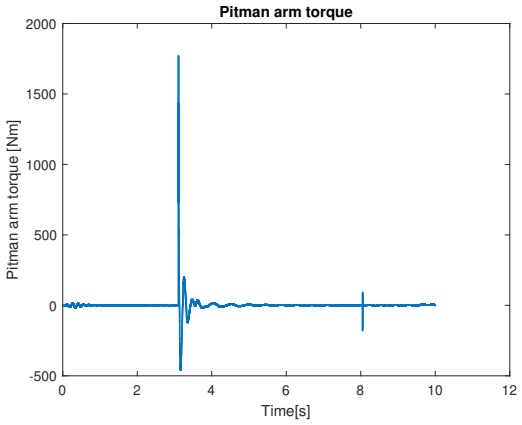

(c) Pitman arm torque

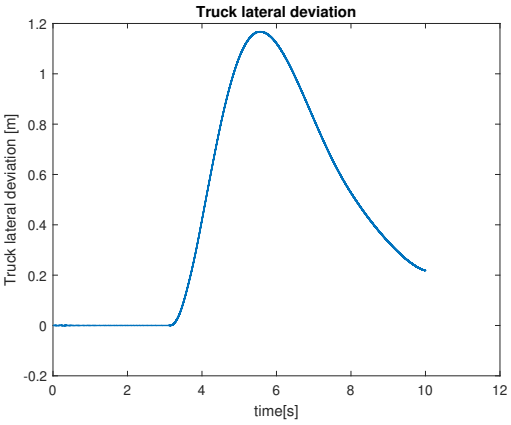

(d) Lateral deviation

Figure 5.4: EHPS with wheel lock

5.2.1.3 EPS on figure 8 track

This trial has both the boost and controller disabled which yields a reference for future trials with controller and for this maneuver.

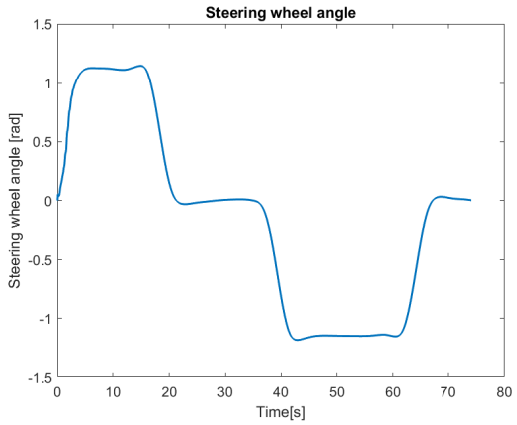

(a) Steering wheel angle

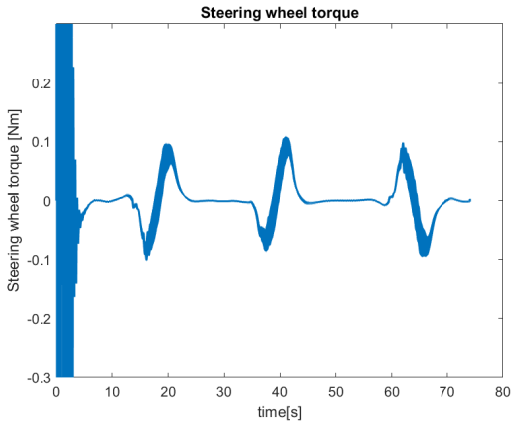

(b) Steering wheel torque

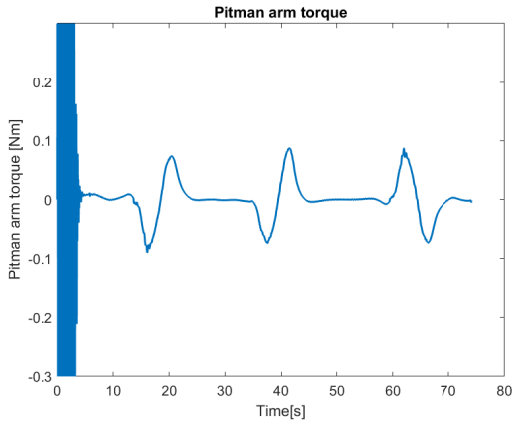

(c) Pitman arm torque

Figure 5.5: EPS on figure 8 track

5.2.1.4 EPS with wheel lock

This trial has both the boost and controller disabled which yields a reference for trials with the controller while performing this same maneuver.

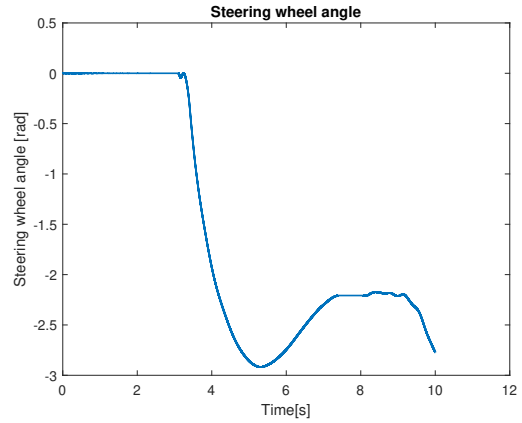

(a) Steering wheel angle

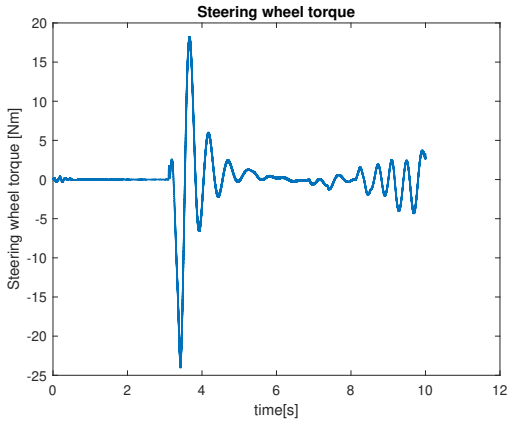

(b) Steering wheel torque

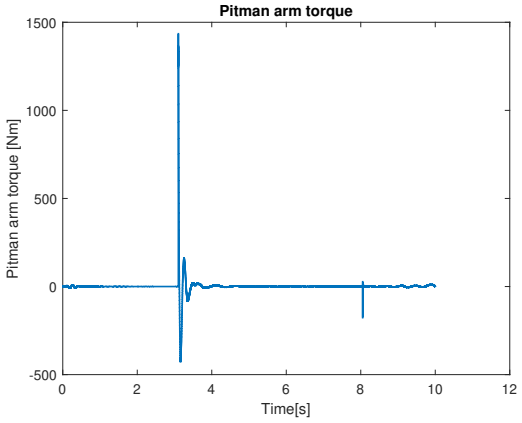

(c) Pitman arm torque

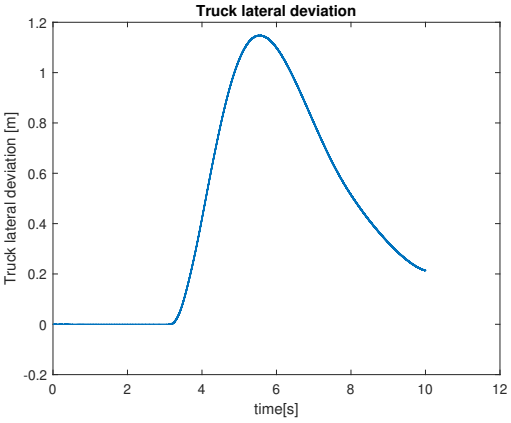

(d) Lateral deviation

Figure 5.6: EPS with wheel lock

5.2.1.5 EPS and boost on figure 8 track

This trial depicts the contribution of boost to assist driver in negotiating the figure 8 maneuver.
The torque plots show oscillation in the intervals where the steering wheel angle is almost a constant value. This interval is where the torque needed to assist is zero or very small. Since the assist request is a very small value close to zero, the motor controller becomes unstable and causes the oscillation.

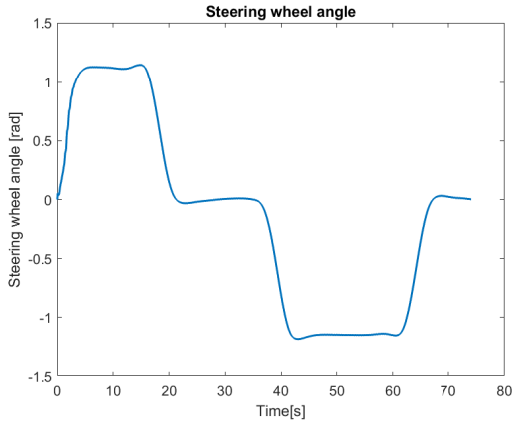

(a) Steering wheel angle

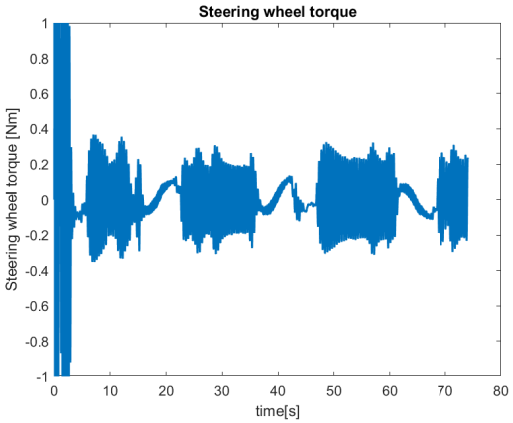

(b) Steering wheel torque

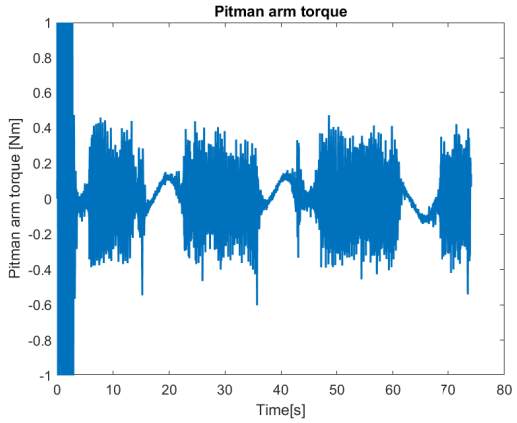

(c) Pitman arm torque

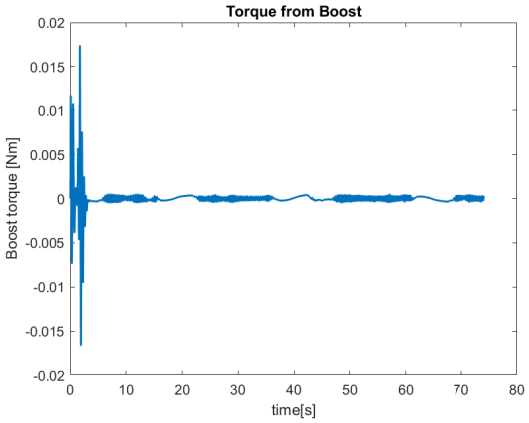

(d) Boost torque

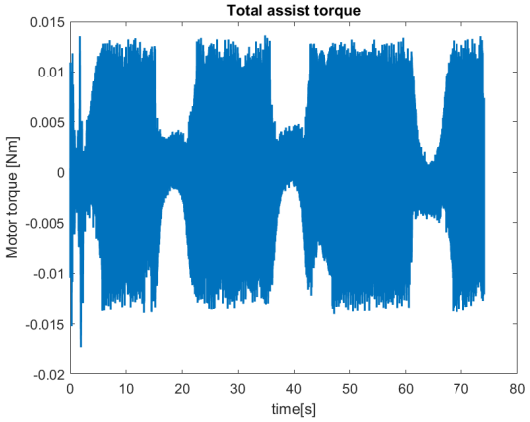

(e) Assist torque

Figure 5.7: EPS and boost on figure 8 track

5.2.1.6 EPS and boost with wheel lock

This trial depicts the contribution of boost to assist driver in overcoming the wheel lock.

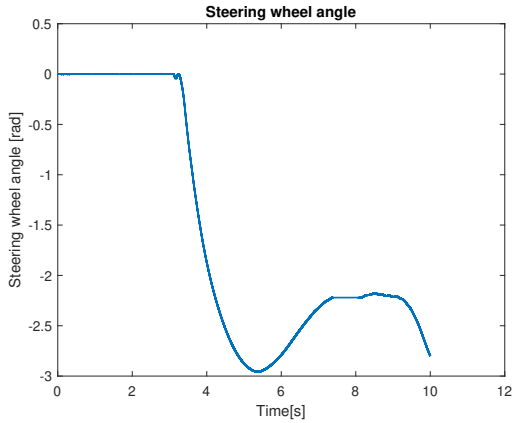

(a) Steering wheel angle

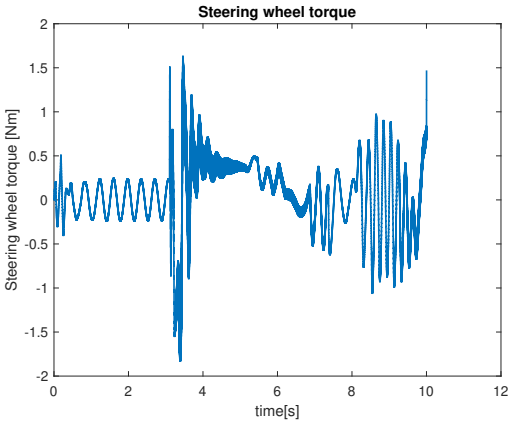

(b) Steering wheel torque

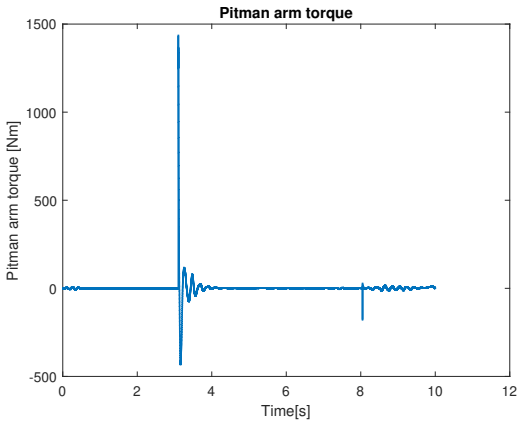

(c) Pitman arm torque

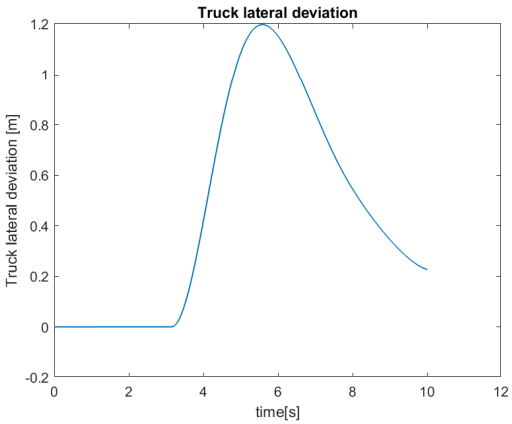

(d) Lateral deviation

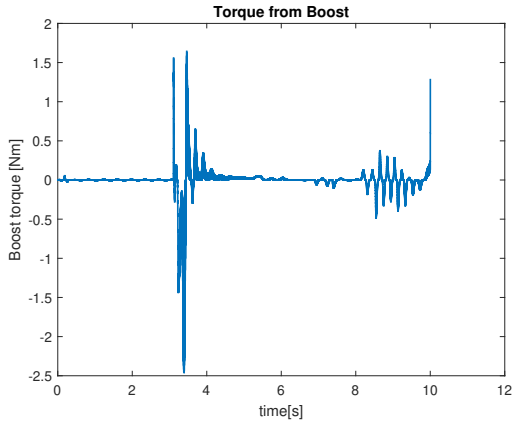

(e) Boost torque

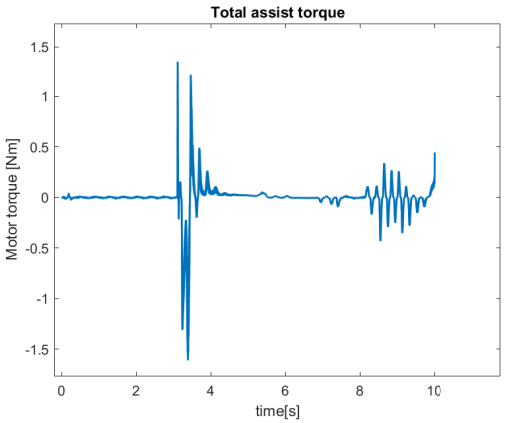

(f) Assist torque

Figure 5.8: EPS and boost with wheel lock

5.2.2 Performance with the controller

This setup can be treated as a closed-loop test where `Steering Controller` as seen in figure 1.6 is enabled. For the EPS topology however, the boost is also considered as can be seen later. The torque-assist from the motor thus adds to the steering effort complementing the driver.

5.2.2.1 EHPS with controller on figure 8 track

This trial depicts the contribution of controller to assist driver in the figure 8 track.

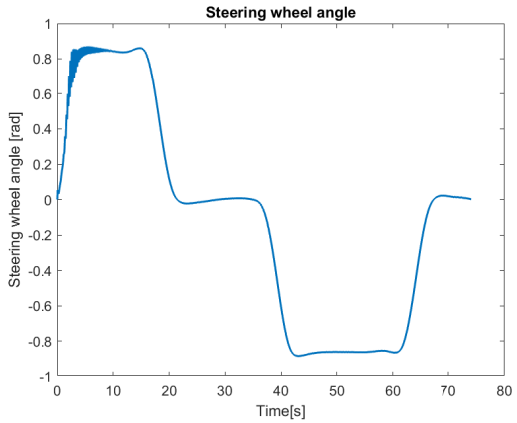

(a) Steering wheel angle

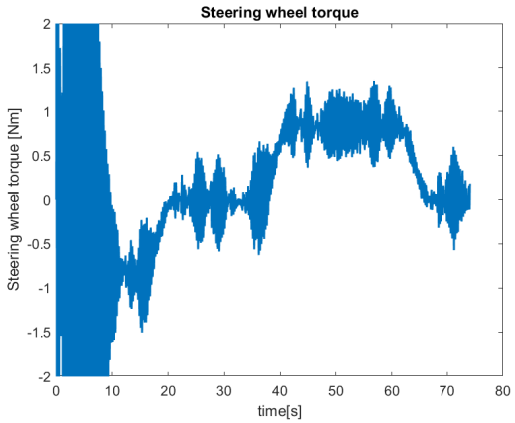

(b) Steering wheel torque

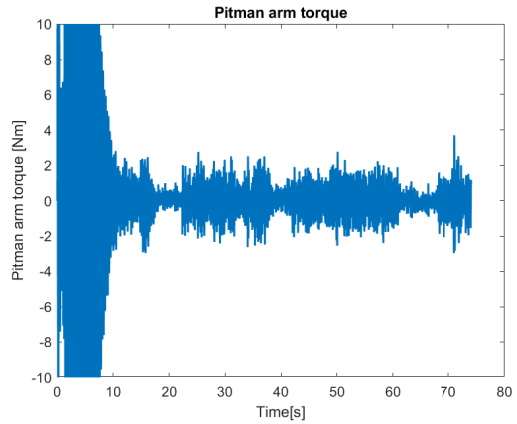

(c) Pitman arm torque

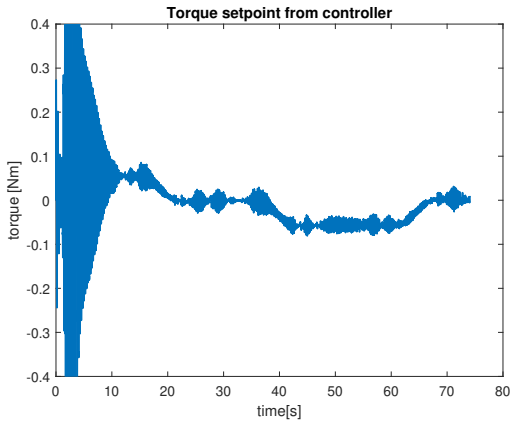

(d) Torque reference from controller

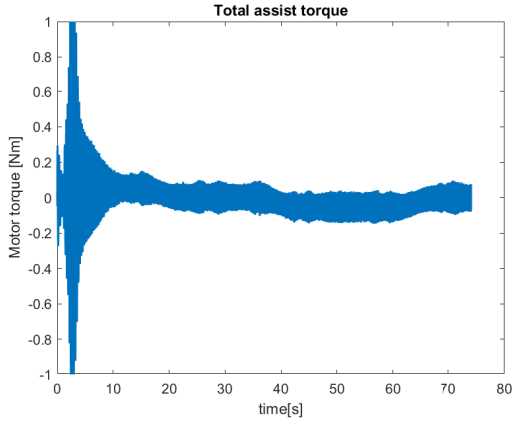

(e) Total assist torque

Figure 5.9: EHPS with controller on figure 8 track

5.2.2.2 EPS with boost and controller on figure 8 track

This trial depicts the contribution of boost and controller to assist driver in the figure 8 track.

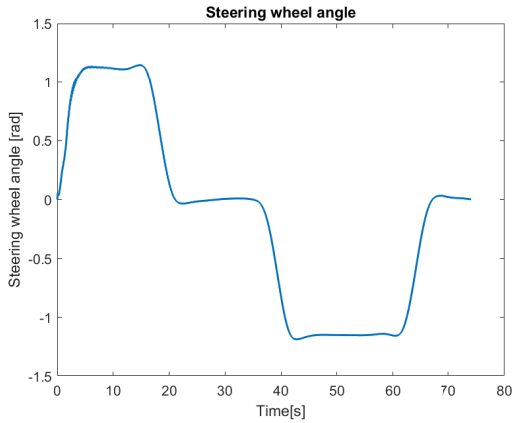

(a) Steering wheel angle

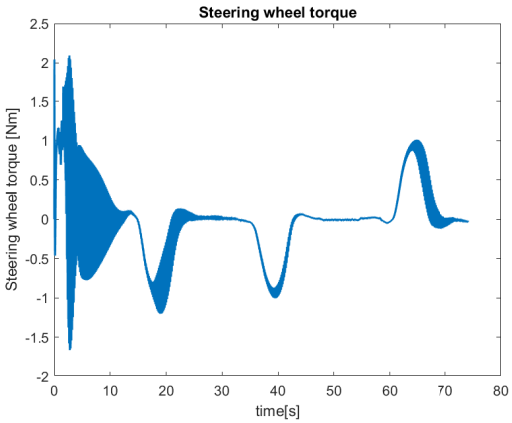

(b) Steering wheel torque

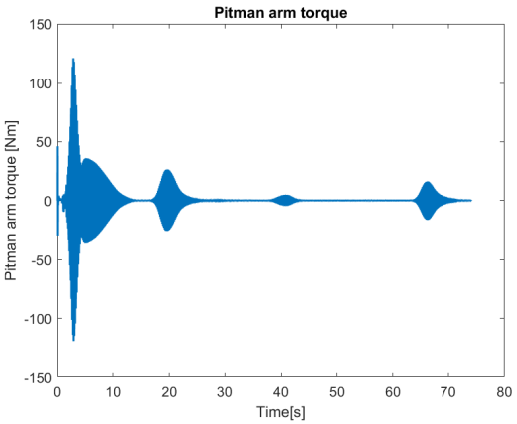

(c) Pitman arm torque

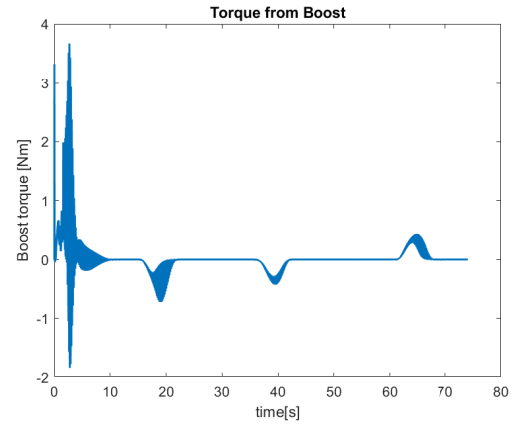

(d) Boost torque

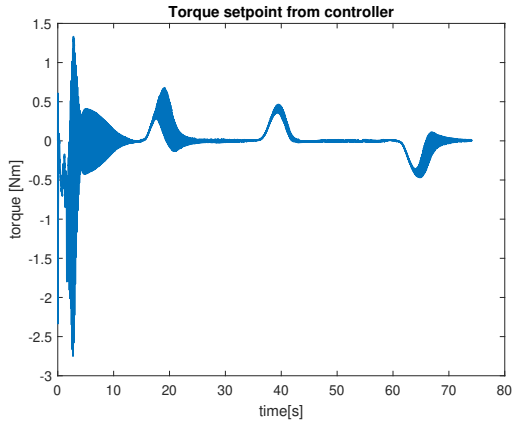

(e) Torque reference from controller

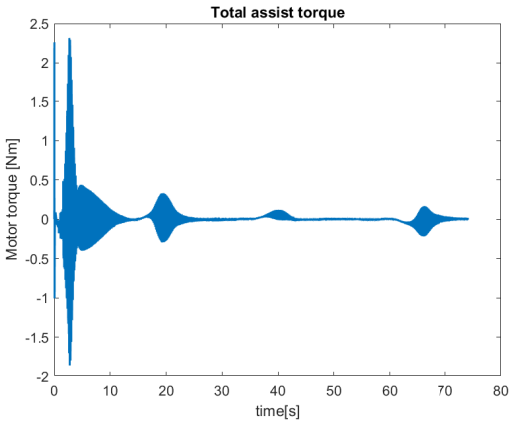

(f) Total assist torque

Figure 5.10: EPS with boost and controller on figure 8 track

5.2.2.3 EHPS with controller during wheel lock

This trial depicts the contribution of the controller to assist driver during the wheel lock scenario.

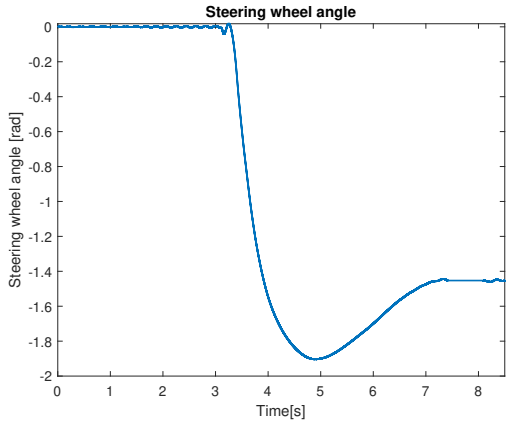

(a) Steering wheel angle

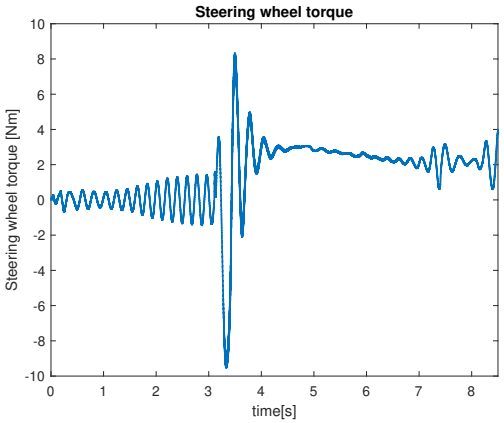

(b) Steering wheel torque

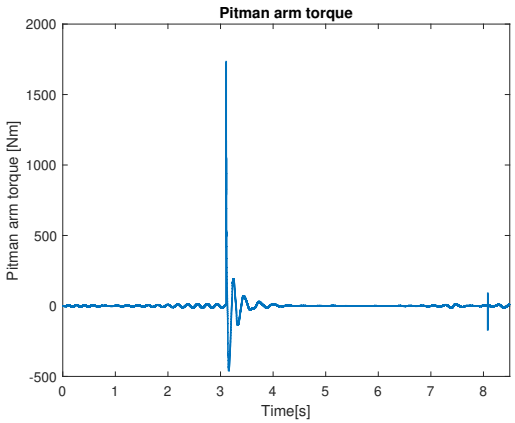

(c) Pitman arm torque

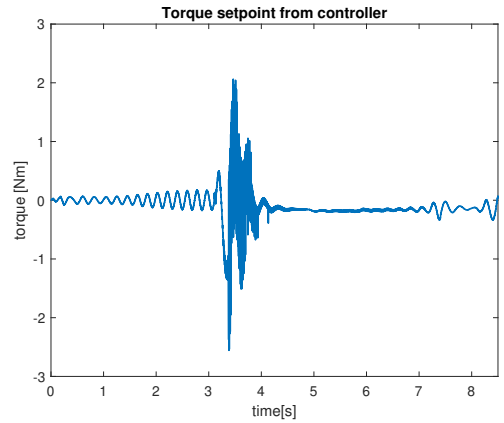

(d) Torque reference from controller

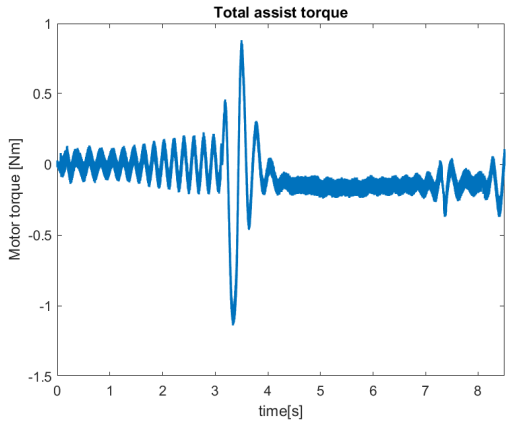

(e) Total assist torque

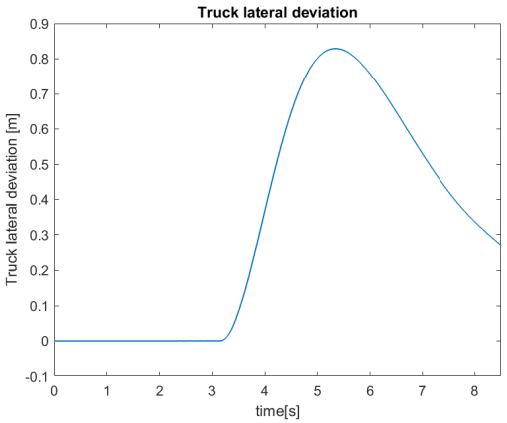

(f) Lateral deviation

Figure 5.11: EHPS with controller during wheel lock

5.2.2.4 EPS with boost and controller with wheel lock

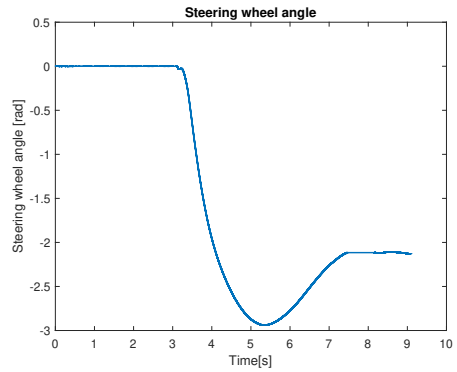

(a) Steering wheel angle

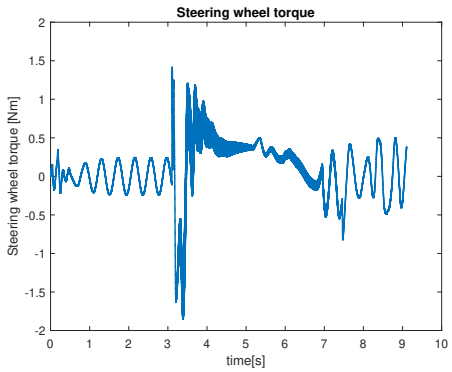

(b) Steering wheel torque

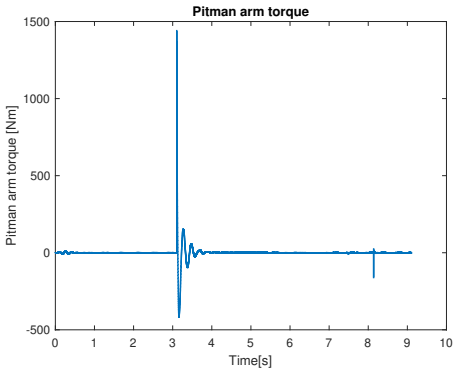

(c) Pitman arm torque

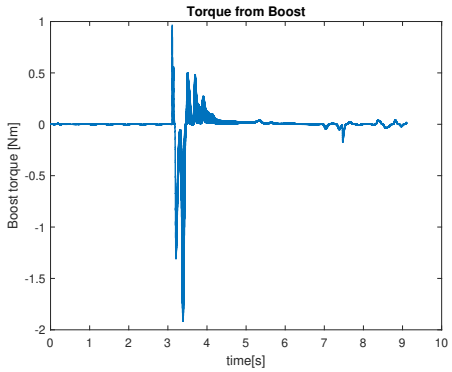

(d) Boost torque

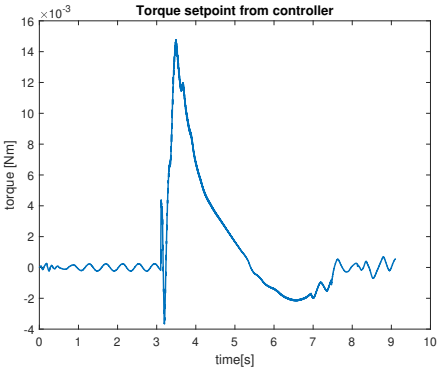

(e) Torque reference from controller

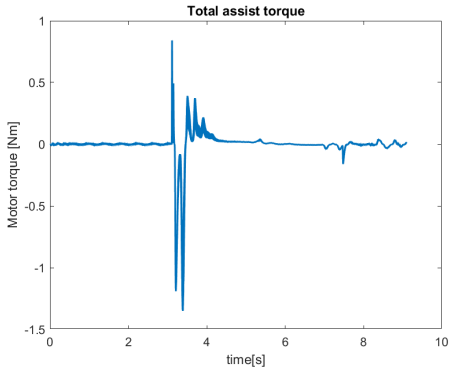

(f) Total assist torque

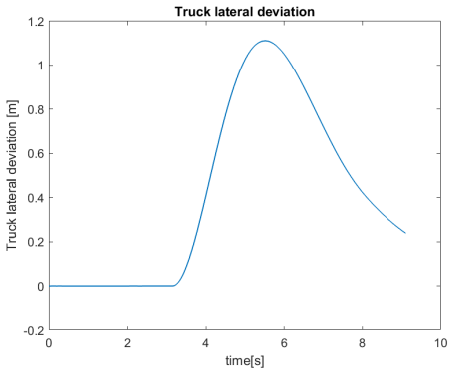

(g) Lateral deviation

Figure 5.12: EPS with boost and controller with wheel lock

6
Discussion and Conclusions

The work presented in this thesis report shows how modelling (with Dymola, Simulink and TruckMaker) and simulation (with TruckMaker) can be used for the development of steering systems and virtual verification of steering feel.
The conclusion here is structured to briefly link the work presented in the earlier chapters to the stated objectives.

6.1 Modelling of the systems and dynamics

The model-based approach for the development of the VDS-like and EPS topologies based on models described in [14] using the Dymola software proved to be a good platform for virtual development. Though assumptions and simplifications were considered, the end model was functional and as anticipated. Modelling the systems included the development of custom components like the `torsion bar` and the `hydraulic gearbox` which exhibit non-linear behaviour. These custom components proved to be crucial in developing high-fidelity steering models and thus successfully capture the system dynamics.

6.2 Analytical conclusions about the steering model on comparison with ground truth FMU

Following the assumptions and limitations discussed pertaining to modelling in the earlier chapters, and the comparison between the ground truth FMU and the developed FMU of the steering system, it can be concluded that the behavior of the developed FMU was largely similar to the former.
However, the torques, specifically the steering wheel and pitman arm showed considerable deviation. This could likely be rectified by addressing the assumptions and limitations mentioned earlier. As long as the scope of this thesis is considered, the steering model behaved satisfactorily.

6.3 Controller

The $\mathcal{H}_2$ controller was experimented to work for the steering application. The controller which is of type `P-K`, was developed following the standard academic procedure as explained in section 3.1. However, the controller was designed considering

all input signals to be zero, which includes `steering wheel angle`. This makes the controller oppose the driver's maneuvers if the angle is non-zero, thereby generating a torque reference that opposes the driver.
Rectifying this would include an angle reference to the controller which would correct the deviation from the driver's intended path.

6.4 The distinctive performance characteristics

The performance of the steering system was tested with the vehicle in TruckMaker, where the vehicle was maneuvered in the figure 8 track and then a wheel lock scenario.

An important note here is that the comparison of energy consumed by the two steering systems to navigate the test scenarios was not made. This is because the energy consumed by the motors can be determined in both topologies but not the energy consumed by the hydraulics in the EHPS system. Thus, it can be deemed unreasonable to compare just the energy consumed by the motors as opposed to the energy consumed by the EHPS and EPS topologies.

In the open-loop setup as in section 5.2.1, what is common to both the EHPS and EPS topologies is that the steering torque for navigating the figure 8 track is very small whereas during the wheel lock situation, the steering wheel torque exceeds the 4Nm limit. The lateral deviation is however almost 1.2m with the steering wheel angle at the instance of wheel lock, to counter it, is -2.9 rad.
EPS with just the assist from boost however, shows considerable improvement in reducing the steering wheel torque for both the figure 8 and wheel lock maneuver, thus assisting the driver supportively. The other parameters like lateral deviation and steering wheel angle remain unchanged.

The section 5.2.2, which displays results from the closed-loop tests shows that the steering wheel torque is in general greater than open-loop tests. This can be attributed to the torque set-point from the controller acting against the driver as explained in the previous section, thus creating the need for the driver to exert more torque and compensate. The torque from boost however supports the driver but is of smaller magnitude.
Focusing on the wheel lock scenario, EHPS with the controller helps reduce the steering wheel angle to -1.9 rad at the instance of wheel lock with the lateral deviation being restricted to 0.85m. But the steering wheel torque needed to take up the corrective action is well above 4Nm, thus not meeting the expectation.
EPS, on the contrary, during the same wheel lock scenario, restricts the steering wheel torque to within 4Nm but with the entire support of boost and very limited input from the controller.

In summarizing the comparison, EHPS and EPS topologies exhibit similar overall behavior and driver feel. While both systems effectively support the driver, and EPS additionally through boost, a notable issue arises with the controller torque set

point, which opposes the driver. Addressing this issue should be a focal point for future improvements.

6.5 Future work

- Redesign controller to incorporate angle reference generator to correct the deviation from driver intended path. This reference generator can be designed by implementing the yaw rate feedback.
- Design motor controller to support direct torque control as opposed to indirect torque control implemented currently.
- Change to have a single MIMO controller for motor and steering control instead of two separate controllers.
- Retune the boost curve for EPS model to improve driver feel.
- Devise other methods to obtain frequency content for weights of the controller.
- Tune model such that the steering wheel torque of the developed model matches that of ground truth FMU.
- Develop $\mathcal{H}_\infty$ controller for disturbance rejection.

Bibliography

[1] Trafikverket, "Lastbilstrafik 2021," 2021. [Online]. Available: https://www.trafa.se/globalassets/statistik/vagtrafik/lastbilstrafik/2021/lastbilstrafik-2021.pdf.

[2] Volvo Lastvagnar. "Volvo fm – chassispecifikationer," [Online]. Available: https://www.volvotrucks.se/sv-se/trucks/trucks/volvo-fm/specifications/chassis.html#maxfrontaxleload (visited on 01/20/2023).

[3] Volvo Lastvagnar. "Chassispecifikationer för volvo fh," [Online]. Available: https://www.volvotrucks.se/sv-se/trucks/trucks/volvo-fh/specifications/chassis.html (visited on 01/20/2023).

[4] Volvo Lastvagnar. "Chassispecifikationer för volvo fh16," [Online]. Available: https://www.volvotrucks.se/sv-se/trucks/trucks/volvo-fh16/specifications/chassis.html (visited on 01/20/2023).

[5] Scania. "Scania specification p, g and r series," [Online]. Available: https://www.scania.com/content/dam/scanianoe/market/uk/brochures/truck/spec-sheets/r-series/spec-sheet-scania-r520la6x2mna.PDF (visited on 01/20/2023).

[6] Benz. "Actros specification and dimension," [Online]. Available: https://www.mercedes-benz-trucks.com/en_TH/models/long-distance-actros/technical-data/specification-dimension.html (visited on 01/20/2023).

[7] J. W. Durstine, "The truck steering system from hand wheel to road wheel," *SAE Transactions*, vol. 82, pp. 93–150, 1973, ISSN: 0096736X, 25771531. [Online]. Available: http://www.jstor.org/stable/44716303.

[8] C. Morton, C. M. Spargo, and V. Pickert, "Electrified hydraulic power steering system in hybrid electric heavy trucks," *IET Electrical Systems in Transportation*, vol. 4, no. 3, pp. 70–77, 2014. DOI: https://doi.org/10.1049/iet-est.2013.0050. eprint: https://ietresearch.onlinelibrary.wiley.com/doi/pdf/10.1049/iet-est.2013.0050. [Online]. Available: https://ietresearch.onlinelibrary.wiley.com/doi/abs/10.1049/iet-est.2013.0050.

[9] *Fact sheet-dynamic steering*, ENG Version 02, Volvo Trucks, Jun. 2018. [Online]. Available: https://stpi.it.volvo.com/STPIFiles/Volvo/FactSheet/ACTST-TO,%20ASFE-BAS,%20ASFE-OG,%20ASFE-PS,%20ASFE-PO%20%20_Eng_02_309626347.pdf.

[10] *What is electric power steering*, Electrical workbook, Aug. 2022. [Online]. Available: https://electricalworkbook.com/electric-power-steering/.

[11] Wikipedia contributors. "Sustainable development goals — Wikipedia, the free encyclopedia." (2022), [Online]. Available: https://en.wikipedia.org/w/index.php?title=Sustainable_Development_Goals&oldid=1128486799 (visited on 12/20/2022).

[12] J. Parambath. "Environmental effects of hydraulic fluids," [Online]. Available: https://jojibooks.com/2021/09/24/environmental-effects-of-hydraulic-fluids/ (visited on 12/20/2022).

[13] Dassault Systems. "Dymola systems engineering," [Online]. Available: https://www.3ds.com/products-services/catia/products/dymola/ (visited on 08/17/2023).

[14] J. Loof, "Modeling and control of a truck steering-system for active driver support," 2018. [Online]. Available: https://pure.tue.nl/ws/files/90582488/20180219_Loof.pdf (visited on 12/19/2022).

[15] E. Drenth, *Numerical instability in springs connected in series*, Interview, Conducted by Alireza Marzbanrad, Emil Erikmats and Sharath Chandra Ashok Kumar, 2023.

[16] The Modelica Association. "Limit the range of a signal." (Oct. 19, 2019), [Online]. Available: https://doc.modelica.org/Modelica%203.2.3/Resources/helpDymola/Modelica_Blocks_Nonlinear.html#Modelica.Blocks.Nonlinear.Limiter (visited on 08/25/2023).

[17] M. Budimir. "How do gearmotors impact reflected mass inertia from the load?" Motion Control Tips. (Jan. 10, 2019), [Online]. Available: https://www.motioncontroltips.com/how-do-gearmotors-impact-reflected-mass-inertia-from-the-load/ (visited on 08/25/2023).

[18] Dassault systèmes AB. "Fmi support in dymola." (2017), [Online]. Available: https://manualzz.com/doc/o/ps9xq/dymola---dassault-syst%C3%A8mes-exporting-fmus-from-dymola (visited on 08/27/2023).

[19] P. Yedamale, *Brushless dc (bldc) motor fundamentals*, Microchip Technology Inc., 2003. [Online]. Available: http://electrathonoftampabay.org/www/Documents/Motors/Brushless%20DC%20(BLDC)%20Motor%20Fundamentals.pdf.

[20] B. M. Chen, "H2 optimal control,"
in *Encyclopedia of Systems and Control*, J. Baillieul and T. Samad, Eds. London: Springer London, 2013, pp. 1–7, ISBN: 978-1-4471-5102-9. DOI: 10.1007/978-1-4471-5102-9_204-1. [Online]. Available: https://doi.org/10.1007/978-1-4471-5102-9_204-1.

[21] P. Sarala, S. F. Kodad, and B. Sarvesh,
"Analysis of closed loop current controlled bldc motor drive,"
in *2016 International Conference on Electrical, Electronics, and Optimization Techniques (ICEEOT)*, 2016, pp. 1464–1468. DOI: 10.1109/ICEEOT.2016.7754925.

[22] IPG Automotive, "Steering system," in *Carmaker Reference Manual*, ser. Version 11.0.1, ch. 14.

[23] IPG Automotive, "Steering system," in *Truckmaker Reference Manual*, ser. Version 11.0.1, ch. 10.

[24] S. M. Awchar, S. P. Diwan, and P. Arlikar,
"Advanced technique for speed control of sensor-less bldc motor,"
in *2018 Fourth International Conference on Computing Communication Control and Automation (ICCUBEA)*, 2018, pp. 1–5. DOI: 10.1109/ICCUBEA.2018.8697796.

[25] W.-S. Im, W. Liu, and J.-M. Kim,
"Sensorless control of 3-phase bldc motors using dc current model,"
in *2014 IEEE Energy Conversion Congress and Exposition (ECCE)*, 2014, pp. 4484–4490. DOI: 10.1109/ECCE.2014.6954015.

A

Dymola model of Non-linear hydraulic torsion bar spring

The nonlinear hydraulic torsion bar spring was modeled in Dymola as seen below. The parameter values are removed because of confidentiality reasons.

```
model torsion_bar_with_limit4 "Spring with linear and
   nonlinear regions.
  The nonlinear regions can have a discrete offset and a 3rd
      order polynomial
  deflection to torque ratio. "


  extends Modelica.Thermal.HeatTransfer.Interfaces.
     PartialElementaryConditionalHeatPortWithoutT;
  import Modelica.Mechanics.Rotational.Interfaces.Flange_a;
  import Modelica.Mechanics.Rotational.Interfaces.Flange_b;
  import Modelica.Blocks.Types.LimiterHomotopy;
  import Modelica.Units.SI;
  import Modelica.Constants.pi;

  parameter SI.RotationalSpringConstant c_lin(final min=0,
     start=1.0e5) =
    "Spring constant at operational region";
  parameter SI.RotationalSpringConstant c_lin_non = c_lin
    "linear component of nonlinear region";
  parameter Real c_non_3 =
    "3rd order component of nonlinear region";
  parameter SI.RotationalDampingConstant d(final min=0,
     start=0) =
    "Damping constant";
  parameter SI.Angle phi_rel0=0 "Unstretched spring angle";

  parameter SI.Angle delta0 =
    "Maximum deflection";

  parameter LimiterHomotopy
```

```
    homotopyType = Modelica.Blocks.Types.LimiterHomotopy.
      Linear
    "Simplified model for homotopy-based initialization";

  parameter SI.Angle phi_nominal(
    displayUnit="rad",
    min=0.0) = 1e-4 "Nominal value of phi_rel (used for
      scaling)"
    annotation (Dialog(tab="Advanced"));
  parameter StateSelect stateSelect=StateSelect.default
    "Priority to use phi_rel and w_rel as states"
    annotation (HideResult=true, Dialog(tab="Advanced"));

  SI.Angle phi_rel(
    displayUnit="rad",
    start=0,
    stateSelect=stateSelect,
    nominal=if phi_nominal >= Modelica.Constants.eps then
      phi_nominal else
        1) "Relative rotation angle (= flange_b.phi -
          flange_a.phi)";
  SI.AngularVelocity w_rel(start=0, stateSelect=stateSelect)
    "Relative angular velocity (= der(phi_rel))";
  SI.AngularAcceleration a_rel(start=0)
    "Relative angular acceleration (= der(w_rel))";
  SI.Torque tau
    "Torque between flanges (= flange_b.tau)";
  SI.Angle phi_rel_T "Angular deflection due to torque";
  Flange_a flange_a "Flange of left shaft" annotation (
    Placement(
      transformation(extent={{-110,-10},{-90,10}})));
  Flange_b flange_b "Flange of right shaft" annotation (
    Placement(
      transformation(extent={{90,-10},{110,10}})));

protected
  SI.Torque tau_c_lin "Linear spring torque";
  SI.Torque tau_c_non "non-linear spring torque";
  SI.Torque tau_d "Damping torque";
  SI.Torque tau_c_out "Resulting spring torque. Switches
    between tau_c_lin and
    tau_c_non depending on if the deflection is within the
      linear region or
    not";
  Real simplifiedExpr "Simplified expression for homotopy-
    based initialization";
```

```
equation
  phi_rel = flange_b.phi - flange_a.phi;
  w_rel = der(phi_rel);
  a_rel = der(w_rel);
  flange_b.tau = tau;
  flange_a.tau = -tau;

  tau_d = d*w_rel;
  tau = tau_c_out; // + tau_d;
  lossPower = tau_d*w_rel;

  simplifiedExpr = (if homotopyType == Modelica.Blocks.Types
     .LimiterHomotopy.Linear then tau_c_lin
                    else if homotopyType == Modelica.Blocks.
                       Types.LimiterHomotopy.UpperLimit then
                        tau_c_non
                    else if homotopyType == Modelica.Blocks.
                       Types.LimiterHomotopy.LowerLimit then
                        tau_c_non
                    else 0);

  phi_rel_T = phi_rel - phi_rel0;
  tau_c_lin = c_lin*phi_rel_T;
  tau_c_non = (if phi_rel_T > 0
               then c_lin_non*phi_rel_T + c_non_3*(phi_rel_T
                   - delta0)^3
               else c_lin_non*phi_rel_T + c_non_3*(phi_rel_T
                   + delta0)^3);
  tau_c_out = homotopy(actual = smooth(0,
    if phi_rel_T > delta0 then tau_c_non
    else if phi_rel_T < -delta0 then tau_c_non
    else tau_c_lin),
    simplified=simplifiedExpr);

    annotation (Evaluate=true, Dialog(group="Initialization
       "),
              Icon(
      coordinateSystem(preserveAspectRatio=true,
        extent={{-100,-100},{100,100}}),
        graphics={
    Line(points
       ={{-80,40},{-60,40},{-45,10},{-15,70},{15,10},{45,70},{60,40},{80,
       },
    Line(points={{-80,40},{-80,-40}}),
    Line(points={{-80,-40},{-50,-40}}),
```

```
      Rectangle(extent={{-50,-10},{40,-70}},
        fillColor={192,192,192},
        fillPattern=FillPattern.Solid),
      Line(points={{40,80},{-40,0}}, thickness=1),
      Line(points={{40,80},{20,80}}, thickness=1),
      Line(points={{40,80},{40,60}}, thickness=1),
      Line(points={{-50,-10},{70,-10}}),
      Line(points={{-50,-70},{70,-70}}),
      Line(points={{40,-40},{80,-40}}),
      Line(points={{80,40},{80,-40}}),
      Line(points={{-90,0},{-80,0}}),
      Line(points={{80,0},{90,0}}),
      Line(points={
{-88.65,-52.58},
{-87.76,-54.05},
{-86.84,-55.51},
{-85.91,-56.95},
{-84.95,-58.37},
{-83.96,-59.78},
{-82.95,-61.17},
{-81.92,-62.55},
{-80.87,-63.90},
{-79.79,-65.24},
{-78.69,-66.56},
{-77.57,-67.86},
{-76.43,-69.15},
{-75.27,-70.41},
{-74.09,-71.66},
{-72.88,-72.88},
{-71.66,-74.09},
{-70.41,-75.27},
{-69.15,-76.43},
{-67.86,-77.57},
{-66.56,-78.69},
{-65.24,-79.79},
{-63.90,-80.87},
{-62.55,-81.92},
{-61.17,-82.95},
{-59.78,-83.96},
{-58.37,-84.95},
{-56.95,-85.91},
{-55.51,-86.84},
{-54.05,-87.76},
{-52.58,-88.65}}, thickness = 0.5),
Line(points={
{-88.65,-52.58},
```

```
{-100.65,-64.58}}, thickness = 0.5),
Line(points={
{-72.88,-72.88},
{-99.00,-99.00}}, thickness = 0.5),
Line(points={
{-52.58,-88.65},
{-64.58,-100.65}}, thickness = 0.5),
    Text(extent={{-190,110},{190,70}},
      textColor={0,0,255},
      textString="%name"),
    Line(visible=useHeatPort,
      points={{-100,-100},{-100,-55},{-5,-55}},
      color={191,0,0},
      pattern=LinePattern.Dot)}), Diagram(
        coordinateSystem(preserveAspectRatio=false)));
end torsion_bar_with_limit4;
```

B

Model export code

B.1 FMU generation

Below is the code used to generate FMUs from the Dymola models using the Dymola 2022 built in function. `translateModelFMU()`.

```
// Script to linearize all models
clearlog
LogStateSelection:=true;
t_names_modelica = {"topologyA", "topologyC"}; // Topology
   names (topology A / C)
c_names_modelica = {"steer_by_angle", "steer_by_torque"};
   // Control strategy names (steer by angle / torque)
p_names_modelica = {"tau", "w"};       // Power bond names (
   torque / angular velocity)
t_names_matlab = {"topA", "topC"}; // Topology names (
   topology A / C)
c_names_matlab = {"sba", "sbt"};    // Control strategy names
    (steer by angle / torque)
p_names_matlab = {"tau", "w"};       // Power bond names (
   torque / angular velocity)
mod_names_modelica = {{{"",""},{"",""}},{{"",""},{"",""}}};
mod_names_matlab = {{{"",""},{"",""}},{{"",""},{"",""}}};
lin_success = false;

for t in 1 : size(t_names_modelica, 1) loop
    for c in 1 : size(c_names_modelica, 1) loop
        for p in 1 : size(p_names_modelica, 1) loop
            mod_names_modelica[t, c, p] = t_names_modelica[t
               ] + "_" + c_names_modelica[c] + "_" +
               p_names_modelica[p];
            mod_names_matlab[t, c, p] = t_names_matlab[t] +
               "_" + c_names_matlab[c] + "_" +
               p_names_matlab[p];
            DymolaCommands.SimulatorAPI.translateModelFMU("
               topology_models." + t_names_modelica[t] + "."
                + mod_names_modelica[t, c, p], modelName="
               FMU_" + mod_names_matlab[t, c, p], fmiVersion
```

```
                ="2", fmiType="csSolver");
        end for;
    end for;
end for;
```

B.2 Model linearization

To linearize the Dymola models, most of the code from the FMU generation was reused. The differences are the main function used, `linearizeModel()` and the VDS-like model, called `topologyA_lin` which was used instead of `topologyA`.

```
// Script to linearize all models
clearlog
LogStateSelection:=true;
t_names_modelica = {"topologyA", "topologyC"}; // Topology
   names (topology A / C)
c_names_modelica = {"steer_by_angle", "steer_by_torque"};
   // Control strategy names (steer by angle / torque)
p_names_modelica = {"tau", "w"};      // Power bond names (
   torque / angular velocity)
t_names_matlab = {"topA", "topC"}; // Topology names (
   topology A / C)
c_names_matlab = {"sba", "sbt"};    // Control strategy names
    (steer by angle / torque)
p_names_matlab = {"tau", "w"};      // Power bond names (
   torque / angular velocity)
mod_names_modelica = {{{"",""},{"",""}},{{"",""},{"",""}}};
mod_names_matlab = {{{"",""},{"",""}},{{"",""},{"",""}}};
lin_success = false;

for t in 1 : size(t_names_modelica, 1) loop
    for c in 1 : size(c_names_modelica, 1) loop
        for p in 1 : size(p_names_modelica, 1) loop
            mod_names_modelica[t, c, p] = t_names_modelica[t
               ] + "_" + c_names_modelica[c] + "_" +
               p_names_modelica[p];
            mod_names_matlab[t, c, p] = t_names_matlab[t] +
               "_" + c_names_matlab[c] + "_" +
               p_names_matlab[p];
            if t == 1 then
                lin_success = DymolaCommands.SimulatorAPI.
                   linearizeModel("topology_models.
                   topologyA_lin." + mod_names_modelica[t, c
                   , p], tolerance=1e-6, resultFile="dslin_"
                    + mod_names_matlab[t, c, p]);
            elseif t == 2 then
```

```
                lin_success = DymolaCommands.SimulatorAPI.
                    linearizeModel("topology_models.topologyC
                    ." + mod_names_modelica[t, c, p],
                    tolerance=1e-6, resultFile="dslin_" +
                    mod_names_matlab[t, c, p]);
            end if;
        end for;
    end for;
end for;
```

C

Motor specifications

Parameter	Value	Unit
Rated Torque	3	Nm
Rated Speed	3000	rpm
Rated Voltage	48	V
Stator Resistance	0.004	Ω
Stator Inductance	23e-6	H
Inertia	0.002	$kg.m^2$
Voltage Constant	12.81	Vp/krpm
Poles	4	-

Table C.1: Motor parameters for VDS-like topology [24]

Parameter	Value	Unit
Rated Torque	10	Nm
Rated Speed	2000	rpm
Rated Voltage	300	V
Stator Resistance	0.9585	Ω
Stator Inductance	0.0085	H
Inertia	6.329e-3	$kg.m^2$
Damping	303.5e-6	Nm.s
Voltage Constant	153.0584	Vp/krpm
Poles	8	-

Table C.2: Motor parameters for EPS topology [25]

D

Weights for Controller

Parameter	Value	SI unit
LvrTrq	1500	Nm
StwAng	3.5	rad
StwTrq	43	Nm
TBTrqE	43	Nm
wStw	3.2	rad/s
wM	199.7	rad/s
LvrSpeed	0.6	rad/s
TBTrqH	0	Nm
TBang	0.0086	rad
tauLever	1500	Nm
deltaStw	32.2	rad
tauM	3	Nm

Table D.1: Weights for Controller

DEPARTMENT OF ELECTRICAL ENGINEERING
DEPARTMENT OF MECHANICS AND MARITIME SCIENCES
CHALMERS UNIVERSITY OF TECHNOLOGY
Gothenburg, Sweden, www.chalmers.se

CHALMERS
UNIVERSITY OF TECHNOLOGY